3D PRINTING OF BIODEGRADABLE POLY (BUTYLENE ADIPATE – CO – TEREPHTHALATE) / HYDROXYAPATITE NANOCOMPOSITES

A DISSERTATION

SUBMITTED FOR THE

PARTIAL FULFILLMENT OF THE REQUIREMENTS FOR

THE MASTER OF SCIENCE DEGREE IN CHEMISTRY

BY

Arun Acharya

Exam Symbol No. : 705/073

Registration No.: 5-2-37-595-2012

CENTRAL DEPARTMENT OF CHEMISTRY

INSTITUTE OF SCIENCE AND TECHNOLOGY

TRIBHUVAN UNIVERSITY

KIRTIPUR, KATHMANDU

NEPAL

DECEMBER, 2020

BOARD OF EXAMINER AND CERTIFICATE OF APPROVAL

This dissertation entitled "**3D Printing of Biodegradable Poly (butylene adipate – co – terephthalate) / Hydroxyapatite Nanocomposites**" by Arun Acharya under the supervision of supervisor Prof. Dr. Rameshwar Adhikari, Central Department of Chemistry, Tribhuvan University, Nepal, hereby submitted for the partial fulfillment of the Master of Science (M.Sc.) Degree in Chemistry. This dissertation has not been submitted in any other university or institution previously for the award of a degree.

……
Supervisor
Prof. Dr. Rameshwar Adhikari
Central Department of Chemistry
Tribhuvan University

……
Co-supervisor
Mr. Ramesh Puri
Research Centre for Applied Science and Technology
Tribhuvan University

……
Internal Examiner
Asst. Prof. Dr. Kshama Parajuli
Central Department of Chemistry
Tribhuvan University

……
External Examiner
Asst. Prof. Dr. Bhim Prasad Kafle
Department of Chemical Science and Engineering
Kathmandu University

……
Head of Department
Prof. Dr. Ram Chandra Basnyat
Central Department of Chemistry,
Tribhuvan University, Kirtipur
Kathmandu, Nepal

Date: 04-12-2020

RECOMMENDATION LETTER

This is to certify that the dissertation work entitled **"3D Printing of Biodegradable Poly (butylene adipate – co – terephthalate)/ Hydroxyapatite Nanocomposites"** has been carried out by Mr. Arun Acharya as a partial fulfillment for the requirement of M.Sc. Degree in Chemistry under my supervision. To the best of my knowledge, this work has not been submitted to any other degree in this institute.

…….

Supervisor

Prof. Dr. Rameshwar Adhikari

Central Department of Chemistry,

Tribhuvan University, Kirtipur

Kathmandu, Nepal

Date: 04-12-2020

DECLARATION

I, **Arun Acharya,** hereby declare that the work prepared herein is genuine work done originally by me and has not been published submitted elsewhere for the requirement of degree program. Any literature, data or work done by other cited in this dissertation has been given due acknowledgement and listed in the reference section.

……

Arun Acharya

Date: 04-12-2020

ACKNOWLEDGEMENTS

I would like to express my sincere gratitude to my supervisor, Prof. Dr. Rameshwar Adhikari, Central Department of Chemistry, Kirtipur, Kathmandu, Nepal for his constant encouragement and for providing amiable working environment. I would like to offer gratitude to Prof. Dr. Ram Chandra Basnyat, Central Department of Chemistry, Kirtipur, Kathmandu, Nepal for providing me an opportunity to carry out this dissertation work. Also, I would like to thank Prof. Dr. Megh Raj Pokhrel, Prof. Amar Prasad Yadav, Prof. Dr. Moti Lal Sharma, Assoc. Prof. Dr. Achyut Adhikari, Assoc. Prof. Dr. Rajesh Pandit, Ms. Jyoti Giri, Mr. Komal Malla, Mr. Ramesh Puri, Dr. Kamal Sharma and Ms. Aliza Khaniya Sharma.

My sincere thanks to all those who have provided me with experimental training and assistance throughout the course of this study most notable Research Centre for Applied Science and Technology (RECAST), Kirtipur, Kathmandu, Nepal, Mr. Ram Chandra Thapa (Zener Technology, Kupandol, Nepal), Prof. Dr. Takahiro Maruyama (Meijo University, Nagoya, Japan), Dr. Suresh Kumar Dhungel (National Acadamy of Science and Technology, NAST, Kathmandu, Nepal) for his assistance with XRD, Department of Plant Resources, Kathmandu, Nepal for his assistance with FTIR, Mr. Lekha Nath Khatiwada (Department of Customs, Minister of Finance, Nepal).

Last but not the least, I wish to record my own gratitude to my parents, friends and all the research scholars who have directly or indirectly provided me with support throughout this project, most notable Mr. Shiva Prasad Bhattarai, Mr. Amar Sharma Khatiwada, Mr. Bimal Neupane, Ms. Prasamsha Panta, Ms. Sonam Tamang, Mr. Santosh Gaire, Mr. Sujan Shrestha, Mr. Nabin Bhurtel and Ms. Nisha Khanal as well as all the friend for their constant help and support.

ABSTRACT

In this work, the hydroxyapatite (HA) biomaterial from a bio-waste namely the buffalo bone was prepared in simple and environmentally friendly way. It was characterized by Fourier Transform InfraRed (FTIR), X-Ray Diffraction (XRD), Energy Dispersive X-Ray (EDX) and Scanning Electron Microscope (SEM) analyses. The average sizes of the nanoparticles were found in the range 8-41 nm as calculated by Debye-Sherrer's formula. FTIR spectra confirmed the presence of major functional groups (PO_4^{3-} and OH^-) in prepared HA samples, with small additional peaks of carbonate ion (CO_3^{2-}). The SEM micrograph showed the formation of small rod-like crystals in the agglomerated particles were presented in as-dried HA powders with size ranges from 1.75 to 2.72 μm. In addition, the micrographs show morphologies for all samples with fine particles and pore size details ranges from 31.3nm to 101nm provides good agreement to be used in a biomedical application.

To make the nanocomposite, HA was macroscopically uniformly distributed over poly(butylene adipate-co-terephthalate) (PBAT) by solvent casting method with the help of magnetic stirrer. By using nanocomposite, the filament for 3D printer was prepared by Noztek machine. Finally, button like structure was prepared by using 3D printer and it was investigated by water adsorption, Biodegradibility and anti-microbial test. The addition of HA brought improvements in stiffness of PBAT, due to high interactions between the carbonyl groups of the polymer matrix and the hydroxyl groups of HA. As the percentage of HA in composite increased, the water absorption percentage of nano-composite also increased. Also, degradation test showed that weight loss percentage gone to decrease with increased percentage of HA in composite. Therefore, this biomaterial has great potential for applications in regenerative medicine as a support for bone growth.

Keywords: Hydroxyapatite (HA), Crystallinity, Porous, 3D Printing, Solvent Casting, Biodegradability, Water Absorption, Hydrophilicity

ABBREVIATIONS

ACP	Amorphous Calcium Phosphate
ASTM	American Society for Testing and Material
AM	Additive manufacturing
FDM	Focused deposition modeling
FRTP	Fiber-reinforced thermoplastic
HA	Hydroxyapatite
ICDD	International Centre for Diffraction Data
MMT	Montmorillonite
nHA	nano- Hydroxyapatite
OHA	oxyhydroxyapatite
OA	oxyapatite
PLA	Poly Lactic acid
PBAT	Poly(butylene adipate – co – terephthalate)
SEM	Scanning Electron Microscope
UV	Ultraviolet
XRD	X-Ray Diffraction
α- TCP	α- tricalcium phosphate
β -TCP	β -tricalcium phosphate

TABLE OF CONTENTS

LIST OF TABLES

LIST OF FIGURES

CHAPTER 1: INTRODUCTION

1.1 Biodegradable Materials

The majority of practical applications are directly or indirectly associated with polymers and thermoplastic polymers exhibit the properties like light weight, thermal stability, tunable gas as well as water vapor barrier properties and good printability. These properties make polymers as versatile materials suitable for product manufacturing such that as automobile, packaging, agriculture and biomedical applications [1]. In spite of several advantages, most of the plastics are associated with certain serious issues such as disposal of solid waste, and scarcity for raw material. In particular, the solid waste generated by polymers serve as environmental hazards [1]**.**

Biodegradable polymer is originated by alternative to the non-renewable polymer based materials. Biodegradable polymers decompose into carbon dioxide, methane, water, inorganic compounds or biomass via microbial activities within the natural environment'. Bio-based polymers are 'based on renewable resources'. Biodegradable polymers may be bio-based [2]. Biodegradable polymer can be classified into two major categories, natural and synthetic polymer[3][4]. Among naturally derived materials, plant based polysaccharides (e.g., cellulose, alginate, dextran) and animal derived polymers (e.g. collagen, silk, chitosan) have been employed for transient applications due to their intrinsic enzymatic degradability. However, these materials can exhibit high batch-to-batch variation and typically have inherent bioactivity, which can elicit immunogenic response when introduced into the body. Conversely, synthetic polymers typically display more predictable physical properties and degradation profiles that can be chemically engineered, and are typically biologically inert [4]. This synthetic biopolymer is prepared by trans-esterification reaction under controlled conditions and therefore generally exhibit predictable and reproducible properties [3].The biopolymers derived from renewable resources find commercial value particularly in plates, cups, food item wrappers, utensils, trash bags, beverage containers and medical devices etc. Most of the biodegradable materials are manufactured from bio

based feed stocks and easily degradable by microorganisms under controlled environmental conditions [1]. Biodegradable thermoplastic polymers like poly (lactic acid) (PLA), poly(hydroxyl)alkanoate (PHA) and polycaprolactone (PCL) have the capability to fulfill the commercial needs along with environmental sustainability. An example of a non-bio-based polymer that is biodegradable is poly (butyrateadipate-terephthalate) (PBAT). PBAT is a biodegradable polymer, produced from petrochemicals [2].

Poly(butylene adipate–co-terephthalate) (PBAT) is a synthetic polymer based on fossil resources, 100% biodegradable [3][5][6][7][8][6][9], has superior in ductility properties with high elongation at break [8][3][10][6][11], excellent in thermal stability [10], very flexible [3][5][8][7][6][12][13], good impact resistance and heat resistance [7][11][13], has superior toughness [10], good ductibility [11], very brittle [14], high mechanical strength [9], low crystallinity[14] and doesn't have cell toxicity[14]. These properties makes PBAT a promising synthetic polymeric biomaterial for tissue engineering application [9].

PBAT is produced by many different manufacturers and may be known by the brand names ecoflex®, Wango, Ecoworld, Eastar Bio, and Origo-Bi [2]. It is also called poly(butylene adipate-co-terephthalate) and sometimes polybutyrate-adipate-terephthalate (a misnomer) or even just "polybutyrate" [2]. PBAT specifically can be produced by polycondensation reaction of 1,4-butanediol with both adipic and terephthalic acid [3][5][6][11]. Terephthalic acid give rise to high thermal stability and mechanical properties while adipic acid and butanediol impart flexibility and biodegradability [5][11].

It is a biodegradable copolymer which can be degraded by microorganism. So, it is considered a sustainable green polyester [8][10]. The melting point of PBAT is 110^{o}C -120^{o}C [10]. It can be used in several application such as packaging materials, hygiene products, biomedical fields, industrial composting and in tissue engineering [6][3]. Despite of the good background for industrial application of PBAT, this polymer has been very scarcely studied for medical devices due to its poor thermal and mechanical resistance [6][3] and low

bioactivity [13] that limits its access to some sectors such as packaging or bone implants [6].

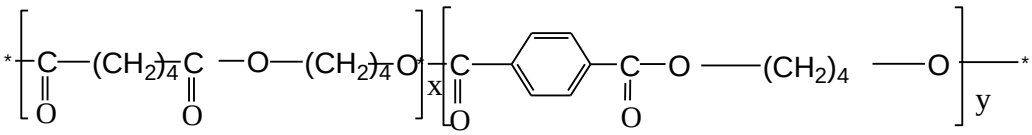

Figure 1.1: Structure of PBAT [3][2]

To overcome these problem, we used filling technique [6][3]. It has been found that the addition of nano-sized filler improved the magnetic, catalytically, optical, electrical, thermal and mechanical properties of PBAT [6].

The combination of PBAT based composites have been reported by several researcher group using different filler such as cellulose nano-crystal (CNC) [3], montmorillonites (MMT), natural fibers, nano-fibrillated cellulose (CNC), red mud, distillers dried grain with soluble (DDGS), and coffee grounds. However, the wear compatibility between the most filler with PBAT is one of the main problem [3].

In this research, we used hydroxyapatite (HA) as a filler concerning to PBAT based nano-composite, only few articles report studies of PBAT/HA nano-composite. In this study, the biodegradable polymer PBAT was combined with the bioactivity and osteoconductive HA to generate scaffolds for potential use in regenerative medicine.

1.2 Biomaterials and Hydroxyapatite (HA)

Biomaterials are materials which have indispensible use in the field of medicine as bone repair and bone tissue engineering. Easy production and good biocompatibility of bio-ceramics make them the most important group of biomaterials[15]. A bioactive material is one which when used as an artificial tissue makes a chemical bond with the natural tissue thus strengthening the implants. The properties of biomaterial for skin tissue engineering are: it should be ingestible and self setting, either in the gel or scaffold form, it should be biodegradable so that the biomaterial degrades in vivo and new skin is formed, it should be biocompatible and not generate immunity responses, it should have

tensile strength near to the tensile strength of skin, it should be flowable and have enough viscosity not to overflow but to fill the wound and finally it should be bioactive [16].

The ceramics that are " specially designed and fabricated for the repair and reconstruction of diseased, damaged, missing or worn out parts of body" is known as Bio-ceramics[15][16]. Depending upon the type of materials, when a synthetic material is placed within the body, tissue reacts with the implanted material in different way. In general, based on the tissue response, biomaterials can be classified as bio-inert, bioactive, or bio-resorbable [17]. Bio-inert bio-ceramics (such as alumina and zirconia) can be described as ceramics that have minimal interaction with the surrounding tissue. Meanwhile, bioactive bio-ceramics refers to ceramics that interact and form a strong interface with the surrounding tissue. Common examples of bioactive bio-ceramics include glasses (silica or phosphate based) calcium phosphate that include hydroxyapatite. Some bio-ceramics are also bio-resorbable materials; which can be described as materials that will be dissolved and gradually replaced by natural tissue, once they are implanted within the human body. Tri-calcium phosphate, calcium carbonate, calcium oxide are common examples of bio-resorbable materials [1][16][17].

The name "apatite" comes from the Greek spelling "apate" which means deceit [17].The reason for this was that the mineral appeared in different colors with a variety of crystal habits, and was thus often mistaken for precious minerals such as aquamarine or amethyst. This variation arises from the fact that the apatite structure has a particularly complex solid system. Apatite is a group of phosphate minerals, usually referring to hydroxyapatite, fluorapatite and chlorapatite, with high concentration of OH^-, F^-, Cl^- ions, respectively in the crystal. The formula of the admixture of the four most common end members is written as $Ca_{10}(PO_4)_6(OH,F,Cl)_2$ and the crystal unit cell formulae of the individual minerals are written as $Ca_{10}(PO_4)_6(OH)_2$, $Ca_{10}(PO_4)_6(F)_2$ and $Ca_{10}(PO)_4(Cl)_2$ [17][18]. Apatite is one of a few minerals having varying Ca/P ratios which are produced and used by biological micro-environmental systems. Apatite is the defining minerals for 5 on the Mohr Scale. Hydroxyapatite, also known as hydroxylapatite, is the major component of tooth enamel and bone

mineral. A relative rare form of apatite in which most of the OH groups are absent and containing many carbonate and acid phosphate substitutions is a large component of bone material. The molar ratio of Ca/P varies from 1.2 almost 2 in HA [17]. The stoichiometric molar ratio of 1.67 [16]. However this is not the value observed in the organism because small amount of material such as C, N, Fe, and another element are incorporated [18].

HA is a major mineral component of calcified tissue (bone and teeth). About 30% of the a cellular part of the bone consist of organic components and 70% of salts [19]. The stands of collagen gives bone its tensile length, and the interspersed crystals of hydroxyapatite give bone its compressional strength. The inorganic composition of bone is primarily formed from salts of calcium and phosphate, the major salt being hydroxyapatite. The ratio of calcium to phosphate varying between 1.3 and 2.0 (per weight) and trace minerals such as magnesium, potassium, sodium and carbonate also being found [9][19] .

HA possesses exceptional biocompatibility and unique bioactivity, no toxicity, inflammatory, pyrogenetic responses and it was similar to naturally occurring HA on the basis of crystallographic and chemical studies[20][21][22][13] [14][23][24]. Naturally, occurring HA is hexagonal in structure with the chemical formula of one unit cell being $Ca_{10}(PO_4)_6(OH)_2$ [19][25][26][27].

Hydroxyapatite is the most emerging bio-ceramics used in various bio-medical applications, mainly in orthopedics and density such as treatment of ostomyletis, osteoporosis, oseous cancer etc. due to its close similarity with inorganic minerals component of bone and teeth [23][25][28][9,11]. It has excellent fibrous tissue formation between implants and bone, and has ability to bond directly to the host bone. HA has also been studied for other non-medical application. For example; coating of HA is often applied to metallic implants, especially stainless steel and titanium alloys to improve the surface properties as well as packing media for column chromatography, gas sensor and catalyst. One of the most important aspects in the application of these materials is the interaction that may exist at the interface with living tissues, both in terms of toxicity, such as dissolution and the active roles that promote the formation of new bone [18].

Hydroxyapatitie biomaterials are materials that are very widely used in several health purposes, including as a source of calcium for manufacturing of toothpaste, used in medicine and oral biology due to the apatite-like structure of enamel, dentine and bone, usually called hard tissue, as an important materials in the formation bone repair. The raw material for the production of hydroxyapatite biomaterial is very easily available and abundant in Nepal. The production process was easy and the cost is also relatively inexpensive if done on a large scale. Among the abundant raw materials are the shells of crabs, shells of egg, scale of fish , bone of buffalo and pig etc [24].

1.3 Tissue Engineering

Tissue engineering is the application of knowledge and expertise from a multidisciplinary field. These are used to develop and manufacture therapeutic products by the combination of matrix scaffolds with feasible human cell systems or cell responsive biomolecules to repair, restoration, regeneration of cells or tissues damaged by injury or disease [21][29]. The concept of three-dimensional scaffolds has certain advantages in the field of tissue engineering over direct cell injection to the tissues. Some of which are (i) It may replace the missing or damaged tissue or injured bone and provide temporary support for self or implanted cells, (ii) we can control the size, shape, strength and composition of the graft in vitro by using tissue engineering, and (iii) it can provides a solution to the problem of bone defects [21][30]. The mechanical properties of the scaffold should be match with native tissue which provides mechanical integrity of the forming tissue and support in vivo-like mechano-transduction between cells and their environment [21][30][31].

Every year, millions of people suffer from bone defects and bone loss which is arising from trauma, tumour or bone diseases, and many of them dying because of insufficient bone substitute and this problem provides numerous opportunities to improve medicine. The treatment of fracture non-union and bone loss associated with trauma, cancer and revision joint arthroplasty problem has become increasingly for orthopaedic surgeons and remains a significant challenge in the field of musculoskeletal injury and there are over several million orthopaedic procedures performed each year [21][31]. The global

orthopaedic market is estimated by Espicom to have been worth approximately US$37.1 billion in 2008, following a growth of 9.7 percent per year [21]. To solve these problems, synthetic and natural polymeric Nano fibrous scaffolds are the alternative for bone tissue engineering applications.

The development of biomaterials made of biodegradable polymer and HA has been extensively investigated to create biological substitutes to regenerate and repair bone tissue [14]. The bone tissue is a natural nano-composites material formed by an organic collagenous matrix and inorganic salts (HA crystals) which provides mechanical support, vital organs protection, phosphate and calcium reservation for the human body [14]. The intrinsic regeneration capacity of the bone without leaving scars is well known. However, in some cases, when the bone defect exceeds a critical dimension healing is compromised and an autologous or allogenic transplant is necessary [14].

The greatest potential for bone substitution is shown by materials based on HA, which can develop tight bonding with bone tissue, exhibits bioactive properties, osteoconductivity, osteoinductive , chemical and crystallographic similarities with bone and teeth, is stable toward bio-resorption, and has no adverse effects on the human organism [14][13][19]. HA has been used as a bone replacement material for complex or partial bone augmentation, filling of bone and teeth or coating of conventional orthopedic and dental implant [13]. Once obtained porous HA objects, molded with different shapes, it is vitally important to have control of manufacture processes of parts or objects so they have mechanical properties suitable for biomedical applications [18]. Currently, bio-composites with HA incorporated as either a filler or coating (or both) into a biodegradable polymer matrix in the form of particle or fibers are increasingly considered for using as bone tissue engineering scaffolds owing to their improved physical, biological and mechanical properties [21].

1.4 Research Objectives

The general objective of this work is 3D printing of biodegradable poly (butylene adipate – co – terephthalate)/ hydroxyapatite nanocomposites.

The specific objectives of this work are as follows:

- To prepare the hydroxyapatite (HA) biomaterial from a bio-waste namely the buffalo bone.
- To prepare the PBAT/HA nano-composite by solvent casting method.
- To prepare the biodegradable composite button structures by using 3D printer and characterize their structural, biodegradibility and water absorption properties.

CHAPTER 2: LITERATURE REVIEW

2.1 Additive Manufacturing Technology

3D printing(3D) or additive manufacturing(AM) is a process of making three dimensional object from a digital file [31][20]. The 3D printing techniques have grown in the last decades starting from 1986 when the first stereo lithographic (SLA) system were introduced in practice [32].

3D printers are a new generation machines that can make everyday things [31][20]. They are remarkable because they can produce different kinds of object in different materials, all from same machine [32]. The creation of a 3D printed object is achieved by using additive processes [33]. In an AM process, an object is created by printing successive layers of material until the entire object is created. Each of these layers is a thinly sliced horizontal cross section of the object. This process is called additive process , because it uses materials more efficiently than traditional; manufacturing techniques, which are subtractive process (such as cutting or drilling) [33]. American Society for Testing and Material (ASTM) international committee F42 on AM technologies defines AM as the process of joining materials to make objects from three dimensional model data, usually layer by layer, as opposed to subtractive manufacturing technologies [34].

3D printing technology has been popular for rapid prototyping technology, which is flexible design by computer aided design software without mold [10]. There is no problem with changing the designing and creating one part at a time [10].

The idea of printing 3D objects conceptualized and patented by Chuck Hull (1986) for making a component by depositing a binder material to selected regions to produce a layer of bonded powder material at this regions [14]. And such steps are repeated for several times to produce successive layers of bonded powder of desired component. The un-bonded powder material is then removed [14]. Utela *et al.* (2008) presented a process of organizing the 3DP implementation into five steps (powder formulation, binder method selection,

binder formulation and testing, printing process specification, and post-processing specification) and presented a review of the literature on 3DP implementation [15].

Berman (2012) has examined the characteristics and applications of 3D printing for mass customization. Thompson provided an overview of the major advancements, challenges and physical attributes related to Direct Laser Deposition (DLD) process [16]. Based on the ability to produce a standard component, D.A. Roberson *et al.* (2013) have evaluated the capability of five desktop additive manufacturing (AM) machines [17]. Merissa Piazza provided the summary of the literature about additive manufacturing[34].

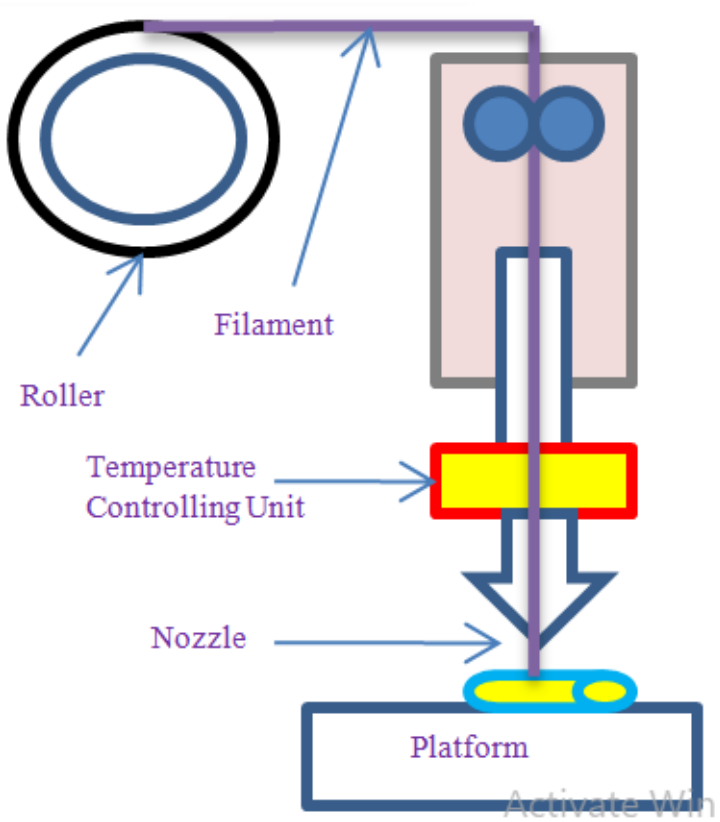

Figure 2.1: 3D Printer

Huang *et al.*(2013) has also reviewed the societal impact of additive manufacturing in (1) customized healthcare due to improve quality of people health, (2) reduced environmental impact for manufacturing sustainability, (3) simplified supply chain to increase efficiency [18]. Lee and Kim (2015)

analyzed trend of 3D printing-related patents to investigate patent application trends by country by assignee and technology [19]. Singh *et al.* (2015) reviewed the recent technological advancements in materials and in technological aspects of 3D printing, identified future challenges and potential applications in engineering, manufacturing and tissue engineering [20].

Currently, nine types of 3D printers were commercialized, [32]

1. Stereo lithography (SLA)
2. Digital light processing (DLP)
3. Fused deposition modeling (FDM)
4. Selective laser sintering (SLS)
5. Selective laser melting (SLM)
6. Digital beam melting (DBM)
7. Laminated object manufacturing (LOM)
8. Binder Jetting (BJ)
9. Material Jetting (MJ)

Among them, FDM technology is currently the most popular 3D printing technology. 3D printers which use FDM technology construct object layer by layer from the very bottom up by the heating and extruding thermoplastic filament [10][33]. Among all 3D printing techniques, FDM is good one because it doesn't require the use of any solvent and offer great simplicity and flexibility in material handling and processing [33]. Use of FDM also reduce material residence time in the heating step and allows continuous production and is quite cheap [35].

FDM is the only 3D printing technology which uses production grade thermoplastics, so items printed have excellent mechanical, thermal and chemical attributes. It is a common 3D printing (3DP) techniques used for the free form fabrication of complex shapes based on polymer [5]. FDM techniques mostly based on polymer in the filament form [10].

Figure 2.2: Different type of 3D Printer [32]

However, it can also be use the raw feed stock materials in the pellet form which drastically reduces the material cost but the production of uniform filament is time consuming and relatively expensive [10]. In addition to thermoplastic, a printer may extrude support material too. Then, the printers heat thermoplastic until its melting point and extrude it throughout nozzle on a printing bed. FDM allows for the depositing material via a nozzle.

The slicer software running on the computer connected to the 3D printers translate the measurement of an object into x, y and z co-ordinates and control the nozzle and the foundation follow calculated route during printing [10]. When the thin layer of plastic binds to the layer beneath it, it melts and hardens. When the layer is completed, the base is lowered to accommodate the printing of the next layer [32]. The support materials can be easily removed by hand with a cutting tool; however, there is a risk to leave impression on the surface requiring an additional polishing on order to obtain a good quality printing. The risk of damaging model, loosing details or break the geometry is readily high [32]. The quality of the 3D printed object depends upon the additive material composition, the manufacturing process, the type of 3D printer used, the speed of printer and volume of object printed [33].

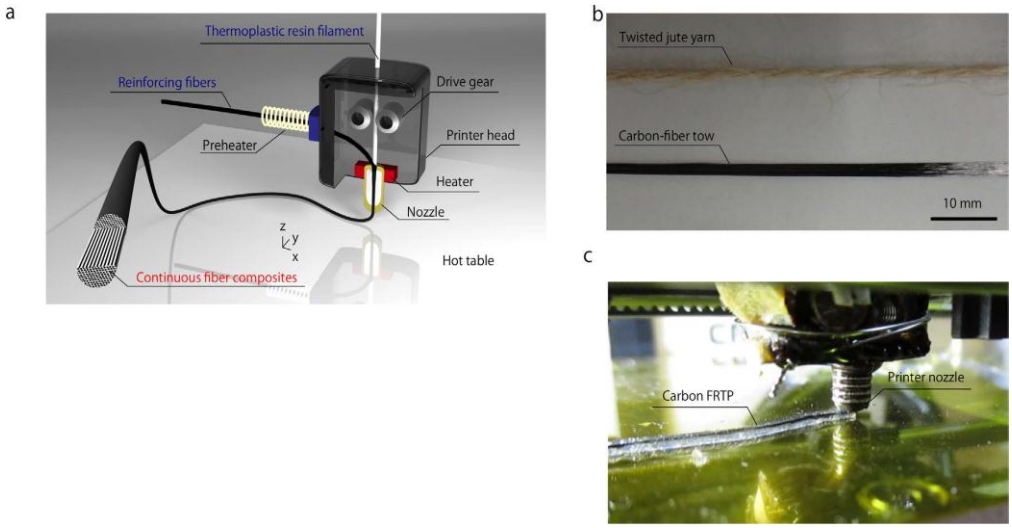

Figure 2.3: (a) Schematic of the 3D printer head used to produce continuous FRTPs using in-nozzle impregnation based on FDM. (b) Continuous fiber reinforcements used for 3D printing. (c) Photograph of the 3D printing of a CFRTP [36].

Up to date, the development in 3DP technology in various application is further required such as small parts or pseudo organs in the medical industry, new fashion clothes in the textile industry, automotive , manufacturing aerospace, pharma and healthcare, retail , military engineering, biotech, Jewelry. Eye wear. Geographic information system, sport and construction parts [10][20][37][31]. Recently, it was used in medicine and tissue engineering application as well [31][38][39].

3DP techniques gives a big opportunity to help Pharmaceutical and medical companies to create more specific drugs, enabling a rapid production of medical implant and changing the way that doctors and surgeon plan procedures [32]. 3D bio-printing is solution to generate the path of patient specific tissue and organs than when the patient need a donor and several different tissue including bone, skin, cartilage, muscle and neural by the help of 3D printing.

Venugopal *et al*. (2010) constructed 3D model through computer-aided design or modelling software. This include selective laser sintering (SLS), stereolithography (SLA), fused deposition modelling (FDM) and direct metal laser sintering (DMLS) [21]. In the context of tissue engineering, this provides a paradigm leap. The precision, reproducibility and ability to construct a unique and patient specific implant are the success of this method [21].

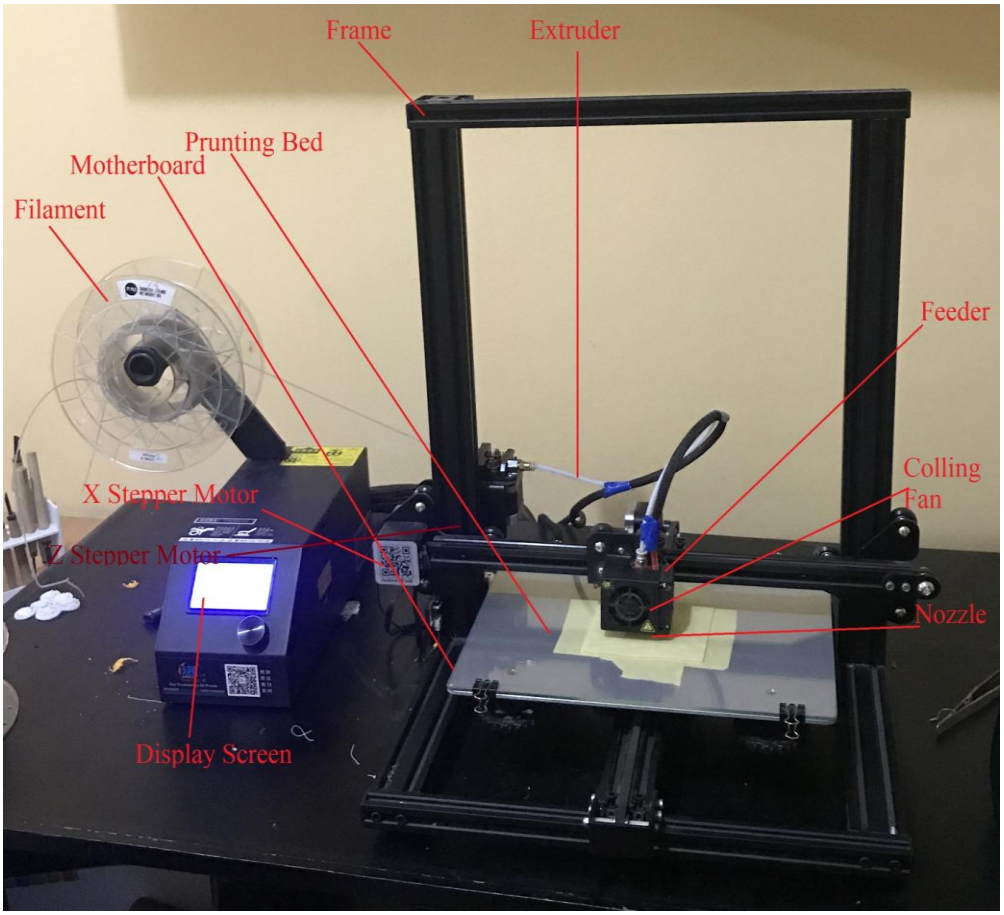

Figure 2.4: Name of different parts used in 3D Printer

The more porous and flexible scaffolds is more likely which allows the integration and proliferation of cells. Shaunak *et al.* (2014) focused on conventional method of construction of scaffolds namely particulate leaching, freeze drying, foaming, emulsification, thermally induced phase separation and electro spinning. The main problem of these technologies was the inability to control shape, porosity and adequate biochemical properties [21]. Robotic Assisted deposition is a composite scaffold which was made by the combination of PLA and polycaprolactone with HA content up to 70% by weight. However, composite inks was prepared by using a toxic solvent i.e. dichloromethane.

Among all 3D technique, focused deposition modeling (FDM) which does not use of any solvent and offer great simplicity and flexibility in material handling process. It also reduces the material residence time in heating step and allows continuous production [22]. PBAT is extensively used biodegradable polymer for the fabrication of medical implant device and tissue engineering scaffold. Gruyter (2017) focused a method to obtain the high quality composition for

FDM, filament requires a high quality composite, high stiffness, low melting viscosity and good powder dispersion[40]. Fused deposition modeling is an extrusion of 3DP process, mostly based on polymer in the filament form [5].

The drawbacks of 3DP technology deal with low mechanical properties, long processing time, conflicting mass production scale, poor dimensional stability due to thermal induced volume shrinkage and heat distortion of material [10].

2.2 Filaments

3DP filaments are the thermoplastic feedstock for fused deposition modeling 3D printer. Once heated to the room temperature, thermoplastic become flexible and that allows the printer to sculpt the filament to create your shapes before it cools down. Filament size depends on the sizes of nozzle used in the 3D printers. Most common nozzle sizes are 0.4mm, 0.35mm and 0.25mm. For this, common filament sizes are 1.75mm and 2.85mm in diameter.

The common types of filament used in 3D printers are [8][10][6][14]:

1. Acrylonitrile Butadiene Styrene (ABS) 3D filament
2. Poly Lactic acid (PLA) 3D Filament
3. Poly Ethylene Terephthalate (PET) 3D filament
4. Poly Ethylene Trimethylene Terephthalate (PETT) 3D filament
5. Nylon Filament
6. Poly Vinyl Alcohol (PVA) filament
7. Sandstone filament
8. Wood filament
9. Metal filament PLA/ABS
10. High Impact Polystyrene (HIPS) filament
11. Magnetic Iron PLA filament
12. Conductive PLA
13. Carbon fiber 3D printer filament
14. Flexible TPE filament
15. Glow in the dark filament
16. Amphor 3D printer filament
17. Poly(butylene adipate–co-terephthalate) (PBAT) filament

These filament are commonly used because they are tough, impact resistant properties, strength, flexible, biodegradable, 100% recyclable, stable, harmless, easy to print, durable, no unpleasant or harm full odors and with unique properties.

These filaments have different application to make different object and material. Some application of these filaments are: consumer product like plastic, automotive parts, moving parts, kitchen application, electronic housing, various toys, surgical implant including surgically implanted pins, rods, screws, mesh, cups, plates, kitchen, utensils, mechanical components, machine parts, structural parts, home décor and many more application.

The most common thermoplastic filaments in 3DP technology are PLA and ABS, which were derived from bio-based and petroleum based resources [10]. Here, researcher trying to make new type of filament which is flexible and biodegradable. Biodegradable polymer offer a number of advantages to environmental conservation due to their non-harmful effect [3]. These polymeric materials have a crucial role in the world today and they can be found in a variety of application including aerospace, aeronautical, automotive, medical, sensor etc [3].

2.3 Crystal Structure of HA

The general chemical formula of hydroxyapatite is $Ca_{10}(PO_4)_6(OH)_2$ and it has Ca/P ratio of 1.67. The structure of calcium HA is reported by LeGeros *et al.*[41] to have been determined by Beevers and McIntyre [13] and later refined by Kay *et al.*[42]. The unit cell contains Ca^{++}, PO_4^{--} and OH^- ions closely packed together to represent a apatite structure. Most researchers suggest that hydroxyapatite has a hexagonal crystal structure with a space group, $P6_3/m$[41]. This structure can be seen in the figure 2.5. This space group is characterized by the six-fold c-axis perpendicular to three equivalent a-axes (a_1, a_2, a_3) at angles of 120^oC to each other. The ten calcium atom belong to either Ca(I) or Ca(II) subsets depending on their environment. Four calcium atom occupy the Ca(I) positions: two at levels Z=0 and two at Z=0.5[41]. Six calcium atom occupy the Ca(II) position: one group of three calcium atoms describing a

triangle located at Z=0.25, the other group of three at Z=0.75, respectively. The six phosphate (PO_4) tetrahedral are in a helical arrangement from levels Z=0.25 to Z=0.75. The networks of PO_4 groups provide the skeletal frameworks which gives the apatite structure its stability. The oxygen of the phosphate group are described as one O, one O_2 and two O_3[41]. The dimensions of the unit cell at room temperature are: a_o= b_o= 9.11 A^o and C_o=6.86 A^o [15].

The oxygen atom in figure 2.5[a] and in one tetrahedron in figure 2.5[b] have been numbered, and position of the horizontal mirror planes at ¼, ¾ etc, marked on the c-axis.

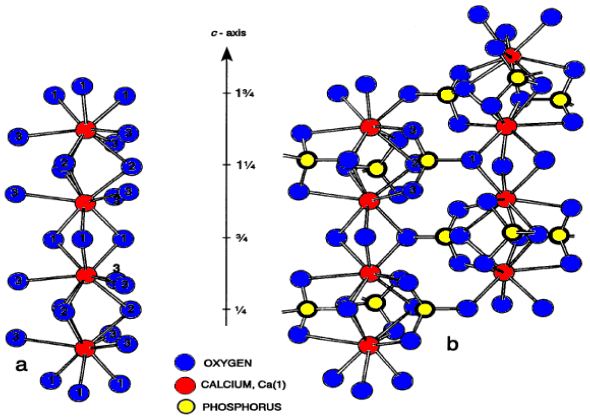

Figure 2.5: Structure of hydroxyapatite a) shows the oxygen co-ordination of columnar Ca (I) ions in apatite b) shows the linking of that column via the PO_4 tetrahedra[13]

The crystallographic structure of pure HA is shown in figure 2.6. This structure allows for the inclusion of substitutional ions, including Na^+, K^+, Mg^+, Sr^+, Cl^-, F^-, CO_3^{2-}, SiO_4^{2-} and HPO_4^{2-}[16]. The presence of substitutional ions distorts the crystal lattice and so reduces crystallinity, resulting increased bioactivity.

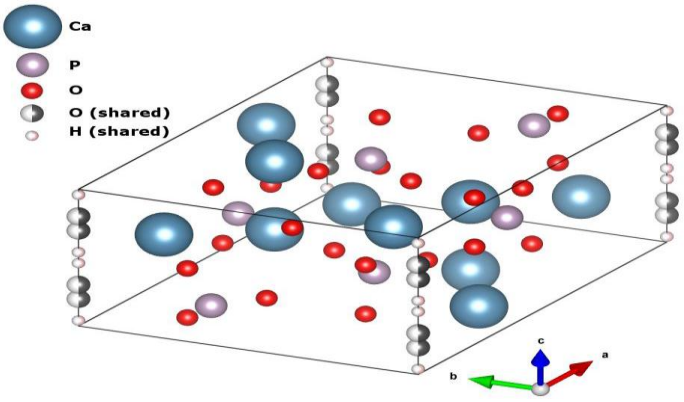

Figure 2.6: Unit cell structure of hydroxyapatite crystal [17]

The micro morphology of HA showed that HA has a short rod-like or rod-like structure; the size of HA ranges from 20 nm to50 nm and the aspect ratio was less than 10. It was seen that a pore structure was distributed on the rod structure with the size of about 2 nm[11].

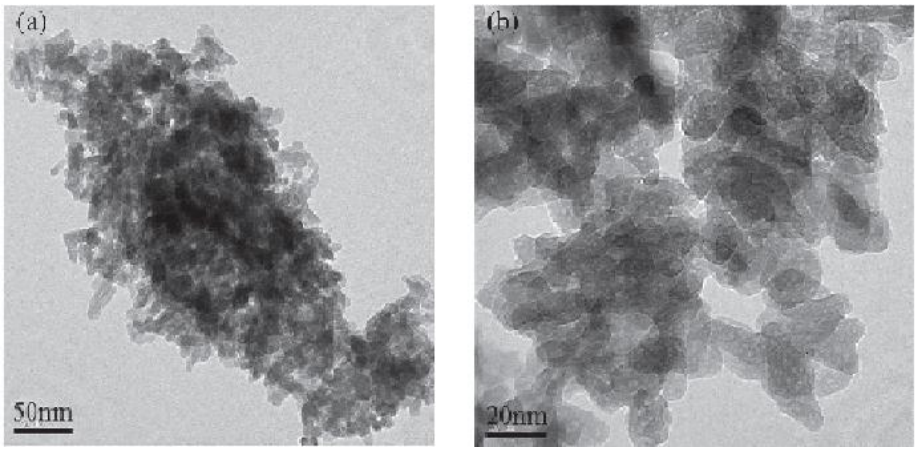

Figure 2.6: TEM image of HA [11]

2.4 Biomedical Application of 3D Printed Nanocomposite

Anna Aimar *et al*. gave a review article on the 3DP in medical field and design needs to think outside the norm for changing the health care [32]. Nowadays, the 3DP technology represent a big opportunity to help pharmaceutical and medical companies to create more specific drugs, enabling a rapid production of medical implants and changing the way that doctors and surgeons plan procedures[32]. Veysi Malkoc introduced the challenges and the future of 3D bio-printing [37]. 3D bio-printing is a path to generate patient specific tissues and organs that when the patient needs a donor and in the time of donor scarcity, it can be a solution to resort. Using 3D bio-printing, researchers were able to construct several different tissues including bone, skin, cartilage, muscle and neural [37]. Mc Alpine *et al*. used 3D bio-printing technology to generate complex anatomical structures with guidance of 3D scanned images of a rats bifurcating sciatic nerve [43]. Wallace *et al.* developed 3D brain like structures that were created in layer by layer by 3D bio-printing. Biomaterials viscosity and cross linking mechanism determines its printability [44]. The choice of cell source also determines the success of the printed construct.

Matsuzaki *et al.* experimented composite fiber materials infused into PLA for 3D printing, targeting better mechanical properties for the printed parts [36]. A FDM printer was modified in order to impregnate the filament with composite fibers during extrusion. The reinforcing fiber was heated using a nichrome wire before it entered the nozzle to enhance the permeation of the fiber bundles with the thermoplastic resin. The heater inside the nozzle, consolidating the reinforcing fibers and the resin in the heating chamber, melts the resin filament. Final results show superior Young's modulus and strengths compared with materials fabricated using commercial 3D printers.

Wei Zhu *et al*. reviewed the prevailing 3D printing techniques and their most recent applications in building tissue constructs [31]. The relatively well-known inkjet and extrusion-based bio-printing was presented with the latest advances in the fields. The two new light-assisted bio-printing techniques, including digital light processing (DLP)-based bio-printing and laser based two photon polymerization (TPP) bio-printing was introduced and 3D bio-printing of vasculature network was particularly discussed for its foremost significance in maintaining tissue viability and promoting functional maturation [31]

Wattanachai Prasong *et al*. studied the superior toughened biodegradable polymer blend composites from PLA, PBAT and nano talc were prepared for alternative materials in 3DP [10]. This showed the excellent dimensional stability and printability and presented high tensile properties of printing products as compared with neat PLA and commercial 3D printing filaments. Bittmann *et al*. prepared PBAT nano-composites reinforced by different types of nano-clays [3]. PBAT based composites with modified bentonite showed the best thermal and mechanical performance at room temperature, which was the temperature of interest for potential packaging applications.

Zormy Nacary Correa Pacheco *et al*. prepared the extruded fibers from poly (lactic acid) (PLA) and poly (butylene adipate-co- terephthalate) (PBAT) added with cinnamon essential oil (CEO) and characterized by hydrolytic degradation [8]. A two- phase system was observed with spherical particles of PBAT embedded in the PLA matrix. The thermal analysis showed partial miscibility between PLA and PBAT. It was found that blend made from PLA/PBAT improved the physical characteristic of the PLA. As the PBAT content

increased, it become more flexible, mechanically, Young's modulus decreased and the elongation at break increased. The result for the hydrolytic degradation showed weight loss percentage for the fibers was below 5% during 12-week process. The most important change with highest percentage change was obtained at 37°C and alkaline medium (pH 8.50). This result suggest that the studied fiber subjected to hydrolytic degradation in real condition for the storage time of 12 weeks and a temperature of 25^{o}C without change in the morphology. From microscopy, the formation of cracks in the fiber surface was evidenced, especially for PLA fibers in alkaline medium at 37 °C. This study showed the importance of the variables that influence the performance of polyester-cinnamon essential oil- based fibers inagro- industrial applications for horticultural product preservation [8].

Ludvik *et al*. investigated the addition of cellulose fibers in PBAT with bentonite clay to improve fiber dispersion and result in a higher water resistance [45].The average modulus of the composite material was reported to be higher than that of the composition without the cellulose fiber. However, the strength and elongation at break displayed the opposite relationship, which could potentially be overcome by surface modifications of the fiber-matrix. It was noted that weak adhesion between the cellulose fiber and the thermoplastic/clay matrix after the drying stage could cause the fiber to clump during processing, unless a special binder was implemented. Yeh *et al*. studied the compatibility, crystallization, and tensile properties of PLA/PBAT blends indifferent proportions produced by melt blending [46]. The results showed PBAT to be effective in increasing the toughness of PLA.

Sarat Singamneni *et al.* focused to establish the feasibility of the combination PBAT-wood flour blend to be processed by extrusion 3DP and establishing the ideal process condition for the best quality of the printing sample [5]. The 95% PBAT and 5% wood flour filler resulted in the optimum response level at the best coalescence, higher strength and ductility level.

Kikku Fukushima *et al*. studied the several nano-composites of PBAT with 5 and 10 wt% of an unmodified and modified montmorillonite, an unmodified and modified fluorohectorite and an unmodified sepiolite were prepared by melt blending for possible industrial and medical application[6]. All nano-composites showed a good level of clay distribution and dispersion into PBAT,

similar increased in the thermal stability of PBAT in nitrogen and air was obtained upon addition of all clays. The addition of all nano-fillers brought the improvements in hardness of PBAT, due to high interaction between the carbonyl group of the polymer matrix and the hydroxyl group. The dynamic and mechanical experiment showed significant increase in E (elasticity) for all nano-composites indicating that addition of clays led to important enhancement in the elastic properties of PBAT matrix.

Mengru Yang *et al*. prepared 3DP filaments of composite and also investigated their properties compared with the injection sample [7]. The tensile strength of 3D printed sample was three times higher than those of injection molded samples. The maximum elongation at break can reach 65% with the increasing of Poly(3-hydroxybutyrate-co-3-hydroxyvalerate) (PHBV) component, the tensile strength of 3D printed sample increased first and then decreased. The tensile strength could reach up to 160 MPa when the component ration was 80/10/10. Elongation at break of printed specimen increased almost constantly with PHBV content except for the printed sample with the ratio at 60/30/10. The presence of PBAT could reduce the brittleness of blend which was demonstrated by the increased impact strength value from 21.09 Jm^{-1} to 50.00 J/m in the case of PLA/PBAT blends at ratio of 75:25.

Carola Esposito Carcione *et al*. investigated the potentiality of 3DP as a manufacturing method to produce as osteogenic hydroxyapatite-polylactic acid bone graft substitute [40]. In the composite, PLA/HA filament, the HA content was homogeneously distributed within the PLA matrix as confirmed by SEM and EDX analyses. Although, a relatively small content of HA was added, the flexural modulus already showed a slight increase if compared with the pure PLA. Finally, clinical images of a maxillary sinus obtained by cone beam computer tomography were properly converted in the suitable format and successfully used to fabricate a real three-dimensional maxillary sinus model using the developed composite material by 3D printing.

The bone tissue was classified as a "composite material", in which the mineral phase supports almost all the mechanical loads and the organic phase (collagen) serves as a binding material, also absorbs impacts, providing flexibility to the bone. So, researcher introduce an organic phase(Gelatin) to the system to mimic the conformation of actual bone tissue[18]. The second phase of organic-

inorganic composite material was obtained in which the inorganic part form a porous structure (made of HA), while the organic phase was chemically attached to it, forming a flexible matrix. SEM micrograph of a taken sample observed the integration of the two phases to form an organic-inorganic composite material based on hydroxyapatite. It was found that the inorganic structure formed by interconnected pores was connected to one another through the organic phase, showing a cellular-type structure, where there are interconnected pores of different sizes in three dimensions. It was found that the presence of the organic phase significantly improve the compressive strength of the samples. The improvement in these properties was of two orders of magnitude, which indicates a synergistic behavior between the two phases.

Stevanovic S *et al*. investigated the fabrication of HA scaffolds with defined macro porosity by means of powder based 3DP [20]. In order to mime natural bone with its elastic collagen structure, the 3D printed structure was post treated by polymeric infiltration. 3D printed HA scaffold in combination with gelatin result in biodegradable scaffolds promising mechanical properties for potential use in regenerative medicine. The compressive strength value with the developed infiltration approach after the sintering process reached up to 12 MPa (usually 0.5-5 MPa) and a decreased porosity depending on the polymer solution and its concentration. The combination of gelatin and HA processed with an optimized 3DP and infiltration method resulted in customizable scaffolds with the most promising mechanical properties. Literature claims that the higher stability can be attributed to crack bridging provided by the applied gelatin coating, which result in increased compressive strength[47].

Qianru Yao *et al*. studied the micro morphology, mechanical, crystallization and permeability properties analysis of HA/PBAT/PLA [11]. The result showed that the PBAT was dispersed uniformly in the HA/PLA matrix in the form of spherical particles and formed many pores and holes. The tensile strength and elongation at break of the composite film were decreased at first and then stabilized with addition of HA content. In addition, tensile strength, elongation at break and modulus of elasticity of HA/PLA composite film were increased by adding 100% PBAT. The addition of HA and PBAT played a synergistic function in improving the crystallinity of composite film.

Neto *et al*. prepared a PBAT and HA nano-particles based bio-composite by electro spinning and spin coating methods [14]. The amount of crystallinity and amount of residual solvent increased with this addition, probably due to adsorption by the nHA. Also, addition of nHA accelerated the crystallization of the PBAT by almost 7^{o}C, probably the nHA surface acted as a nucleation site for PBAT. It can be observed that addition of nHA considerably improved the mechanical properties of composite structure, by increasing 12.7% the elastic modulus, 25.7% the stress at break and 52% the elongation at break. It was shown that these composite scaffolds supported attachment, proliferation and osteogenic differentiation of human adipose stem cells and showed a mild inflammatory response in the direction of in vitro and in vivo results. Also, a decrease in the flux of inflammatory cell was observed due to the osteointegration and osteoinduction properties of nHA and buffered effect on the OH region.

Maria *et al*. prepared the electro spun PBAT matrices in the presence of a conducting polymer, Polypyrrole (PPy) to obtain an electrically conductive nano-scaffold for bone tissue engineering applications [13]. PBAT scaffolds individually or with PPy supported the adhesion and proliferation of MG-63 cells and the cells on both scaffolds synthesized substantial amount of alkaline phosphate indicating osteoblastic differentiation. The Vitro test showed that PBAT and HA were not cytotoxic to MG-63 cell and promoted high cell proliferation rates with the formation of mineralized nodules. For the mechanistic point of view, the loading of HA increased hydrophilicity, which in turn allowed for a better adsorption of proteins and consequent alteration in the phenotypic expression of osteoblasts. This study also explored the combination of PBAT with synthetic nHA (3% and 5% by wt.) was used for bone regeneration.

Aysu Arslan *et al*. synthesized boron doped HA (B-HA) via microwave assisted bio-mimetic precipitation method [9]. The addition of B remarkably enhanced the osteoinductive effect of HA. HA and B-HA containing 3D PBAT scaffolds were fabricated via well electro spinning method. PBAT fibrous matrices were fabricated via wet electro spinning and bio-mimetic HA and B-HA particles were added into the fibrous matrices. Bioactivity of the scaffold was investigated via proliferation and differentiation of hBMSCS (Human bone

marrow aspirate). According to SEM and TEM analysis, PBAT fibers have a smooth and bead free morphology and HA and B-HA were both dispersed in matrix and embedded into fibers.

Composite of PBAT and HA was prepared to increase biodegradibility, hydrophilicity, hardness. mechanical, thermal and bioactivity properties and making material interesting for industrial and bone tissue engineering application. The aim of this work is to prepare the biodegradable polymer composite by using local available resources and making material potentially interesting for tissue engineering and environmental industrial application.

CHAPTER 3: EXPERIMENTAL METHODS

3.1 Materials

Acetone (Merck, India), bovine bone and distilled water were used to prepare HA nano-particle. Dichloromethane (DCM) was used as solvent to prepared nano-composite of HA and PBAT. Tris-buffer (Fischer Scientific, India) was used for the biodegradable test of composite. All chemical are used without any further purification.

3.2 Preparation of 0.5M Tris buffer

60.57g of Tris Buffer (molecular weight 121.14 g/mol) was added to 500mL beaker. Then, 350mL of de-ionized water was added to the beaker. The beaker was stir until the solution was completely dissolved. After that, pH meter was inserted into the beaker to monitored pH of the solution. It should be basic (pH>7.4). So, 12 M HCl was slowly added to the beaker pH of the solution reached to 7.4. Once the pH of the solution was 7.4, then enough de-ionized water was added to raise the volume to 500 mL.

3.3 Preparation of HA nano-particle

Several methods have been utilized for the synthesis of HA including precipitation technique, sol-gel technique, hydrothermal technique, multiple emulsion technique, biometric deposition technique and electro deposition technique and so on. Here, we synthesized HA from buffalo bone by calcinations.

First of all, the femur bone of buffalo was taken and it was boiled and washed with water for three hours to remove bone marrows, all piece of meat, fat and tendon easier. It was boiled continuously in the commercial pressure cooker for 2 hours for defatting and deproteinase process. The bone was then washed with acetone for several times to remove fats and other impurities. The process was followed by sun drying to eliminate organic substances and to avoid soot formation in the material during the heating treatment. The clean dried bones

were grinded in grinding machine. Then, it was sieved with a particle size less than 350 μm. The deproteinised and defatted bone powder was then calcined at 600°C for 3 hours in a muffle furnace. The HA powder was further calcined at 800°C and 1100°C for another 3 hours to study the effect of calcinations at higher temperature. Following this process, the black ash obtained at 600°C was turned into a white granular powder of HA at 800°C and 1100°C [48][49][25]. The photographic images of different stages of HA preparation from animal bone is shown in Figure 3.1.

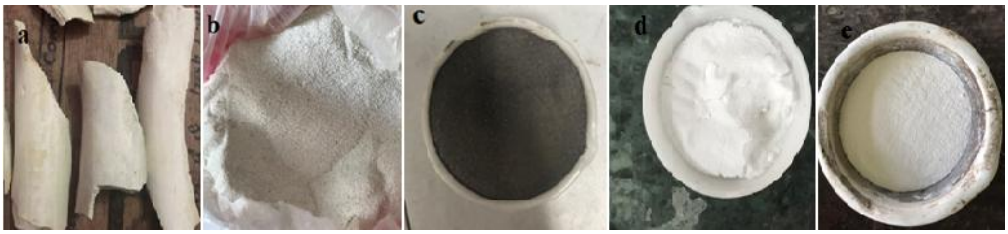

Figure 3.1: Photographs showing the different stages of HA power preparation (a) Femur bone of buffalo (b) crushed buffalo bone (c) powder obtained after calcinations at 600^{o}C (d) powder obtained after calcinations at 800^{o}C (e) powder obtained after calcinations at 1100^{o}C.

3.4 Preparation of Composite

Solvent casting method prepared the HA/PBAT composite films. The detailed steps are as follows. Self-made HA was added to 150 mL CH_2Cl_2 solution containing 40g of PBAT. The additive amount of HA was1 wt%, 1.5 wt%, 2 wt%, 3wt% and 4wt% respectively. After that, the mixed solution was magnetically stirred at room temperature for 2 hour. After the complete homogeneous mixture of HA and PBAT, the solution was poured into a Petri dish and placed at room temperature for 1 days so that organic solvent was evaporated completely. After that, it was placed in an oven at 45^{o}C for 1 hour so that solvent (boiling point of dichloromethane was 39.6^{o}C) was completely removed from the composite. Samples were defined as PBAT, 1% HA/PBAT, 1.5% HA/PBAT, 2% HA/PBAT, 3% HA/PBAT and 4% HA/PBAT [11][9].

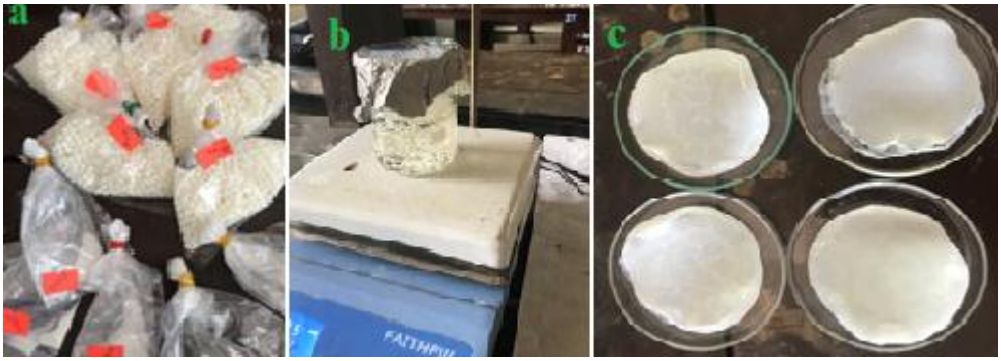

Figure 3.2: Preparation of composite (a) different weight of PBAT and HA was packed in a plastic (b) make a homogeneous mixture of composite by magnetic stirrer (c) thin film of composite placed in a Petri dish [25].

3.5 Preparation of Filament

The filament for the 3D printing process was obtained by melts extrusion. After solvent casting, PBAT was homogeneously coated by HA layer. A filament suitable for 3D printing was obtained by melts extrusion with a twin-screw extruder (Noztek pro filament extruder, Zener technology, Nepal). To obtain a filament with a diameter of $1.75mm^{+}$-0.1mm, two different temperature profiles and screw speeds were used, changing them for pure PBAT and PBAT/HA composite. Different process conditions were tested to optimize the mixing. The optimal parameters, i.e. temperature and screw speed, are listed in Table 3.1.

Table 3.1: Process parameters for the realization of the PBAT and PBAT/HA filaments.

PBAT/HA nanocomposite	Process parameters	Pure PBAT
50	Screw speed(rpm)	40
130	Feed zone temperature, T_1 (°C)	120
135	Metering zone temperature, T_2 (°C)	125

Once the machine was prepared and after reaching the desired temperatures, the polymer composite were slowly fed into the hopper of Noztek machine. As the composite move through the length of the feed chamber the temperature gradually rises and finally the plasticized pool of polymer gets collected in the barrel. Due to the pressure building up from the continuous accumulation, the semi-solid material was extruded from the nozzle tip (1.6 mm diameter).

Initially, the T_1 and T_2 temperature were set to 110^{o}C and 115^{o}C respectively. However, the T_1 and T_2 temperature proved to be insufficient, as the polymer was sticking to the surfaces and causing problems to the screw feeding. As a result, the temperature of the extruder was increased by 5^{o}C intervals until a continuous filament was produced. Immediately at the exit from the extrusion nozzle, the material was air cooled by cooler and coiled on a spool. The average diameter of filament was found to be 1.65 mm [40][8].

Figure 3.3: Preparation of filaments (a) composite of PBAT and HA (b) making filament by using Noztek machine (c) filament with average size 1.65mm coiled on a spool.

3.6 Preparation of 3D object by 3DP

In this experiment, CR 10 mini 3D printer (Zener Technology, Nepal) was used to print the 3D object. First of all in 3D Printing, a blueprint slash three-dimensional digital file of the object was created. Computer Aided Design (CAD) created the digital model. The most commonly used 3D modeling software were Blender, Sketch Up, Auto Cad, Solid Works, Maya, Photo Shop, Thinker Cad or others to create designs. Here, we used Auto Cad software to make a digital file of 3D object. After finished the CAD design, it was time to send it to the printer. First, it was converted into an appropriate file format. The most common 3D Printing file format was called Stereo Lithography (STL). In STL process, 3D File was translated into instructions for the 3D printer to follow. The filament was fitted on the 3D printer. The optimal settings for the critical printing parameters; extrusion temperature, bed temperature, extrusion velocity (spindle speed), print velocity, strand gap, and air gap were identified mainly based on visual inspection during the initial printing process. The nozzle and chamber were both exposed to the atmospheric conditions; hence the actual

temperature inside the chamber may be lowers than the indicated temperature. This would explain the discrepancy between the specified melting temperature from the data sheet and the actual extrusion temperature, which was caused by heat loss from the chamber. The heating element was located only near the botton of the nozzle. The process parameters were listed in the table 3.2 below.

Table 3.2: Building parameters of CR 10 3D Printer

Nozzle size(mm)	**0.4**
Top bottom layer(mm)	4
Layer height(mm)	0.25
Bottom size, length(mm)	30
Infill(%)	20
Flow rate(%)	200
Nozzle temperature(ºC)	130
Bed temperature(ºC)	50

All samples were built according to the parameters reported in Table 3.2. The pure PBAT and the PBAT/HA composites at higher filler content behaved in similar ways in terms of the filament consistency. With time, the polymer develops blockage through the nozzle, either due to the accumulation of the partly solidified mass in the case of pure PBAT or PBAT/HA composite.

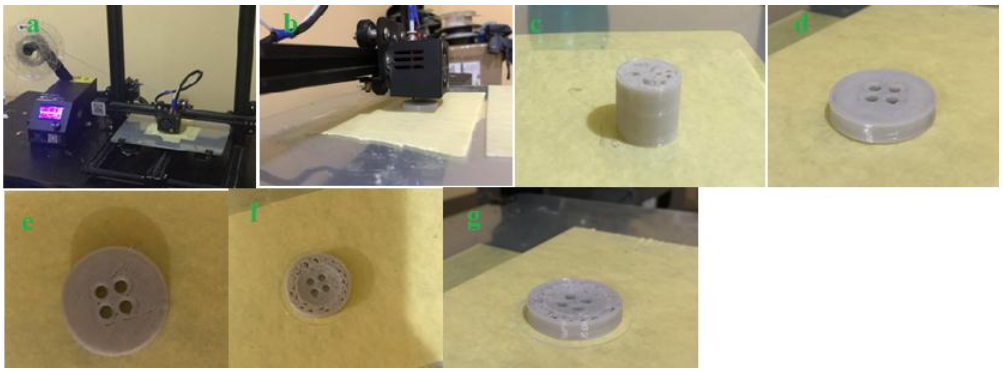

Figure 3.3: 3DP of PBAT and PBAT/HA to make button structure (a) CR 10 mini 3D printer (b) CR 10 mini print the 3D object (c) 3D object made by pure PBAT (d) button structure containing PBAT/ 1% HA (e) button structure containing PBAT/ 1.5% HA (f) button structure containing PBAT/ 2% HA (g) button structure containing PBAT/ 3% HA.

In between, the other two cases at 1% and 1.5% HA filler contents showed the best extrusion characteristics of the polymer composite. However, beyond 2% by weight, solid HA particles aggregate in the nozzle and destabilize the extruded filament characteristics and consequently the printing process. The sample was printed and a sharp needle was inserted into the tip of the nozzle to push the clogged HA particles out. This intermediate cleaning of the nozzle should relieve the built-up pressure of the HA particles, creating an unencumbered path for the filament flow. The results were slightly successful and displayed some improvements in the flow consistency. However, since the material was pushed upwards by the needle, during the resumption of the printing, very little material was deposited initially, requiring some time for the material to regain its flow [8][40].

3.7 Characterization Techniques

3.7.1 X-Ray Diffraction (XRD) Analysis

XRD is an instrumental technique that is usually used to study the crystalline size of materials. The three dimensional structure of non-amorphous materials is defined by regular, repeating planes of atoms, part of the beam is transmitted, part is absorbed by the sample, part is refracted, scattered and part is diffracted. XRD methods for crystalline size determination are applicable for ranges from 2-100 nm. The diffraction peaks are broad for 2-3 mm crystallites while too small broadening for size above 100 nm. Scherrer equation is used for crystallite size determination.

The crystal phase and structure of the samples were determined by X-ray diffractometer (Bruker D2 Phaser) with a monochromatic CuKα radiation source ($\lambda = 0.15418$ nm) at angle 2θ ranging from 20° to 80° at Nepal Academy of Science and Technology (NAST), Nepal. The accelerating voltage of 30 kV and emission current of 10 mA was used.

3.7.2 Fourier Transform Infrared (FTIR) Analysis

The FTIR analysis was carried out in the Department of Plant Resources, Thapathali, Kathmandu, Nepal by using IR Prestige-21 FTIR Spectrometer

(SHIMADZU) and Department of Customs, Minister of Finance, Government of Nepal, Tripureshwor, Kathmandu, Nepal to identify species, functional groups, and vibration modes associated with each peak. Spectra were collected in the spectral range of 4700–400 cm^{-1} using KBr pellet method.

3.7.3 Field Emission Scanning Electron Microscope (FESEM) Analysis

Morphological studies of Hydroxyapatite nano-particles (nano-HA) were established by using field emission scanning electron microscope (Company name: Hitachi and Model number: SU8010) at an accelerating voltage of 15kV. Samples were fixed on SEM stubs with a double-sided carbon tape and they were coated with about 10nm thick layer of gold by sputtering.

3.7.4 Energy Dispersive X-Ray (EDX) Analysis

The EDX analysis (Company name: Shimadzu) was carried out in the Department of Customs, Minister of Finance, Government of Nepal, Tripureshwor, Kathmandu, Nepal to identify different elements present in the sample.

CHAPTER 4: RESULT AND DISCUSSION

4.1 Characterization of HA

4.1.1 X-Ray Diffraction (XRD) Analysis

X-ray Diffraction analysis showed that hydroxyapatite is the only crystalline phase indentified in calcinated bovine bone. The broad peaks suggest that their particles could be of a nano-metric size. It has to be noted, the mineral component of natural bone has been known as poorly crystallized hydroxyapatitie with XRD pattern usually similar to that of synthetic. If the bone was calcined at higher temperature, more organic component is burnt out and the mineral component is re-crystallized. As a result, higher crystallinity is observed. The phase identification of XRD pattern is realized by comparing the experimental XRD pattern to standard complied by the International Centre for Diffraction Data (ICDD) using the cards 00-009-0432 for hexagonal HA structure [50][51]. The well-resolved characteristic peak of highest intensity for HA is obtained at 2θ value of 31.977^{o} corresponding to 211 planes. The phase formed is pure and matches with standard pattern. The standard corresponding plane for HA (100, 101, 200, 002, 202, 301, 130, 131, 113, 203, 222, 132, 321, 004, 240, 241, 502, 323, 511) are well observed in case of synthesized powders [52]. The highest peak obtained at the calcinations process similar to the peak of hydroxyapatite on the JCPDS-09-0432/1996 database. The main (hkl) indices for HA at around 26.5^{o}, 29^{o}, 30^{o}, 26.5^{o}, 29^{o}, 30^{o}, 33^{o}, 34^{o}, 35^{o}, 37^{o}, 40^{o}, 41^{o}, 43^{o}, 48^{o}, 49^{o}, 50.5^{o}, 51.5^{o}, 52.5^{o}, 54^{o}, 65^{o} corresponding to (002), (102), (210), (211), (112), (300), (301), (212), (310), (311), (222), (312), (213), (321), (410), (402), (304) planes [52][53].

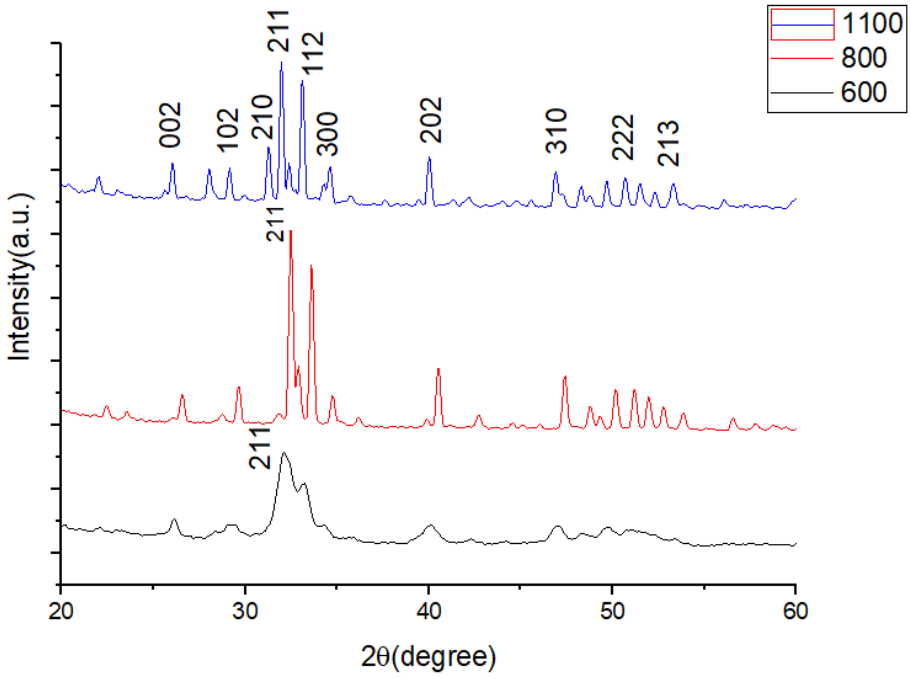

Figure 4.1: XRD patterns of buffalo bone heated at various temperatures (600°C, 800°C and 1100°C)

These diffraction patterns showed a gradual increase in the degree of sharpness of peaks with increasing temperature. These results confirm that effect of heat treatment on the crystal size of hydroxyapatite [51][54][55]. The diffraction pattern (600°C) of the bone ash is very broad which indicates the presence of small crystals of hydroxyapatite. The broader diffraction peaks showed that the sample has small crystallinity or amorphous [56]. With the increase in calcinations temperature from 600°C to 1100°C, narrower and sharper peak is observed. This is due to the complete removal of organic moieties and change of the crystal size of the powder [57]. From the graph, it can be seen that the sample which is obtained at 1100°C has the highest intensity compared to other. The sharper and distinct peak intensity indicates the high degree of crystallinity of HA [56][50][58]. The minor impurity of element is detected at 1100°C. So this calcinations temperature is most suitable to produce the HA.

It should be noted that XRD analysis only provides average crystallite size. As mentioned, the crystallite size influences peak broadening. Thus, changes in peak broadening represent change of the crystallite size distribution. There are some chemical factors, which affect the crystallite size such as denaturing of the bone matrix, release of water (in which the mineral crystals re-crystallize) and

removal of the collagen fibril networks [57]. The sharp intensity and well resolved peaks in XRD patterns at high calcinations temperature prove the complete crystallization.

The crystalline size t_{hkl} of the synthesized nano-HA powder is calculated by using the Debye-Scherrer equation [52][53][59].

$$t_{hkl} = \frac{K\lambda}{B\cos\theta}$$

Where K is the shape factor (K = 0.9 for most of the spherical crystal), λ is wavelength of monochromatic X-ray beam (λ = 1.54056 A^o for CuKα radiation), B is Full Width at Half Maximum (FWHM) of the peak at the maximum intensity, θ is the peak diffraction angle that satisfies Bragg's law for (hkl) plane and t_{hkl} is crystallite size and the symbol h, k and l represent the miller indices and the respective plane is hkl. The crystallite sizes in the powders are tabulated in Table 4.1.

Table 4.1: Calculation of average crystal size of HA prepared at different temperatures

Temperature (^{o}C)	**Peak Position (2θ °)**	**FWHM(2θ °)**	**Crystallite size (nm)**	**Average size (nm)**
600	32.16106	0.9329	8.85	9.75
	33.2098	0.7802	10.64	
800	32.489	0.27207	30.403	32.24
	33.617	0.24353	34.08	
1100	31.97	0.20489	40.33	40.89
	33.11	0.2001	41.45	

The crystal size of HA ranges from 9.75 to 40.89 nm. The average crystal size is small at 600^{o}C and large at 1100^{o}C. The change in crystal size depends on the crystallinity of hydroxyapatite materials. The crystallinity of HA depends on temperature. At higher degree of calcinations, dehydration or removal of water occurs which was confirmed by FTIR [51]. Also agglomeration of particles takes place, which was confirmed by SEM analysis. So, crystallite size increases with increasing temperature, which indicates hydroxyapatite crystals size is affected by temperature during calcinations.

4.1.2 Fourier Transform Infrared (FTIR) Analysis

The synthesized HA is subjected to the FTIR studies in order to confirm the functional groups present in the HA which in turn provides information about the phase purity of the sample synthesized at different temperature. The FTIR spectrum of bone calcinated at temperature about 600ºC, 800ºC and 1100ºC revealed the characteristic peak of HA, which is consistent with some previous reports [49][60][61]. The chemical functionality of the produced HA was investigated based on the functional groups represented in its spectrum. The absence of low intense band at around 2840–2930 cm^{-1} confirm absence of C-H band in the HA. This indicates the complete removal of organic components from the starting material [60][54]. These bands can be divided into three main categories associated with phosphate, carbonate and hydroxyl groups. The band located at 462.92, 563.21, 594.08, 601.79, 956.69, 1010.7 and 1018.41 cm^{-1} are originated by PO_4^{3-} ions [61][16][62][51][57]. The initial formative indicator of hydroxyapatite at all point of sintering (600°C,800°C,1100°C) was in the form of a pronounced broad band around 1000 cm^{-1} to 1100 cm^{-1} which can be ascribed to asymmetric stretching mode of vibration of PO_4 group [60][54]. Also, the band between 563 cm^{-1} to 594 cm^{-1} for all the samples corresponds to symmetric P-O stretching vibration of PO_4 group[60].

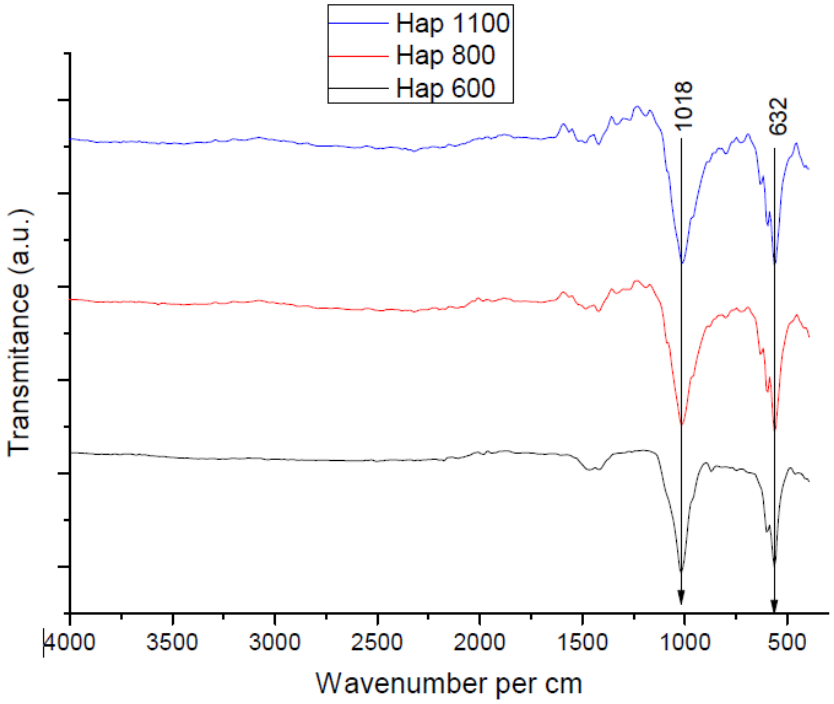

Figure 4.2: FTIR spectra of HA calcined at (a) 600ºC, (b) 800ºC and (c) 1100ºC

Absorbance at 632.65 cm^{-1} is due to the presence of OH^- ion, characteristic of the HA [16][49][51][54][57]. The medium sharp peak at 632.65 cm^{-1} was assigned to the O-H deformation mode and vibrational mode [63][64].

The double-split peaks which appeared at 1465.9 and 1419.61 cm^{-1} at 600ºC and 1481.33 and 1419.61cm^{-1}were related to CO_3^{-2} asymmetric stretching which indicates that CO_3^{-2} actually entered the lattice of the obtained HA [60][49][51][63]. The peak position of carbonate ions in FTIR spectra depends on whether the carbonate ions is substituted for the hydroxyl ion or the phosphate ion in the hydroxyapatite lattice [16]. Carbonate ions are common impurities in both synthetic and natural hydroxyapatite [57]. The samples showed small frequency bands around 2175.7 and 1982.82 cm^{-1} at 600ºC ascribed to the release of CO_2 during heat treatment[61]. The peak at 871.82 cm^{-1}at 600ºC and 802.39 cm^{-1} at 800 and 1100ºC further confirms the ionic substitution of CO_3^{-2} into the HA. This originates from type A carbonate substitution, indicating the presence of surface labile CO_3^{-2} Abifarin et al., 2019). Notably, bones are natural composites comprising mainly of collagen and HA [60]. Many research work demonstrated that calcium phosphates including HA possess a compositional structure which is in many ways similar to natural bones [60]. Therefore, based on the results reported herein, it can be inferred that the HA produced exhibits similar chemical characteristics like the bio-minerals present in calcified human bones. Consequently, it can be exploited for producing materials for bone replacement purposes.

Table 4.2: Different functional group present on HA

Functional group	Wavenumber cm^{-1}	Vibration
PO_4^{-3}	1018.41 cm^{-1} ,964.41 cm^{-1} , 570.93 cm^{-1}	asymmetric stretching symmetric stretching
CO_3^{-2}	1481.33 cm^{-1}	symmetric stretching
OH^{-1}	634 cm^{-1}	Deformational vibrational

4.1.3 Field Emission Scanning Electron Microscope (FESEM) Analysis

The particle size and morphology of calcinated hydroxyapatite powders was confirmed by FESEM analysis. The FESEM images gave insight into the hydroxyapatite structure with respect to particle size and shape. The particles had irregular shapes with edges and corners, rather than being spherical, and most of them were in the range of 1.75 or 2.72 μm in dimensions. This irregular shape of the particles and also their large sizes might be due to incomplete grinding of burnt bone during the production of the bone ash [25]. It should be noted that FESEM image does not show the presence of any amorphous organic material indicating that the organic component of the bone is completely removed (Zakaria,2000) [55].

Small rod-like crystals in the agglomerated particles are present in HA powders. The uniform grain with a narrow size distribution corresponding to the crystallinity improvement of the HA powders after calcinations at 1100°C. It is specifically interesting to note that at 1100^{o}C, the HA revealed reasonable interconnectivity similar to natural bone apatite. Furthermore, it revealed great increment in size compared with other samples. This is due to the high possibility for HA particles to crystallize and grow up at elevated temperature as reported by other researchers [65][60]. The increase in size observed here is in agreement with results of the crystal size and crystallinity obtained through XRD analysis.

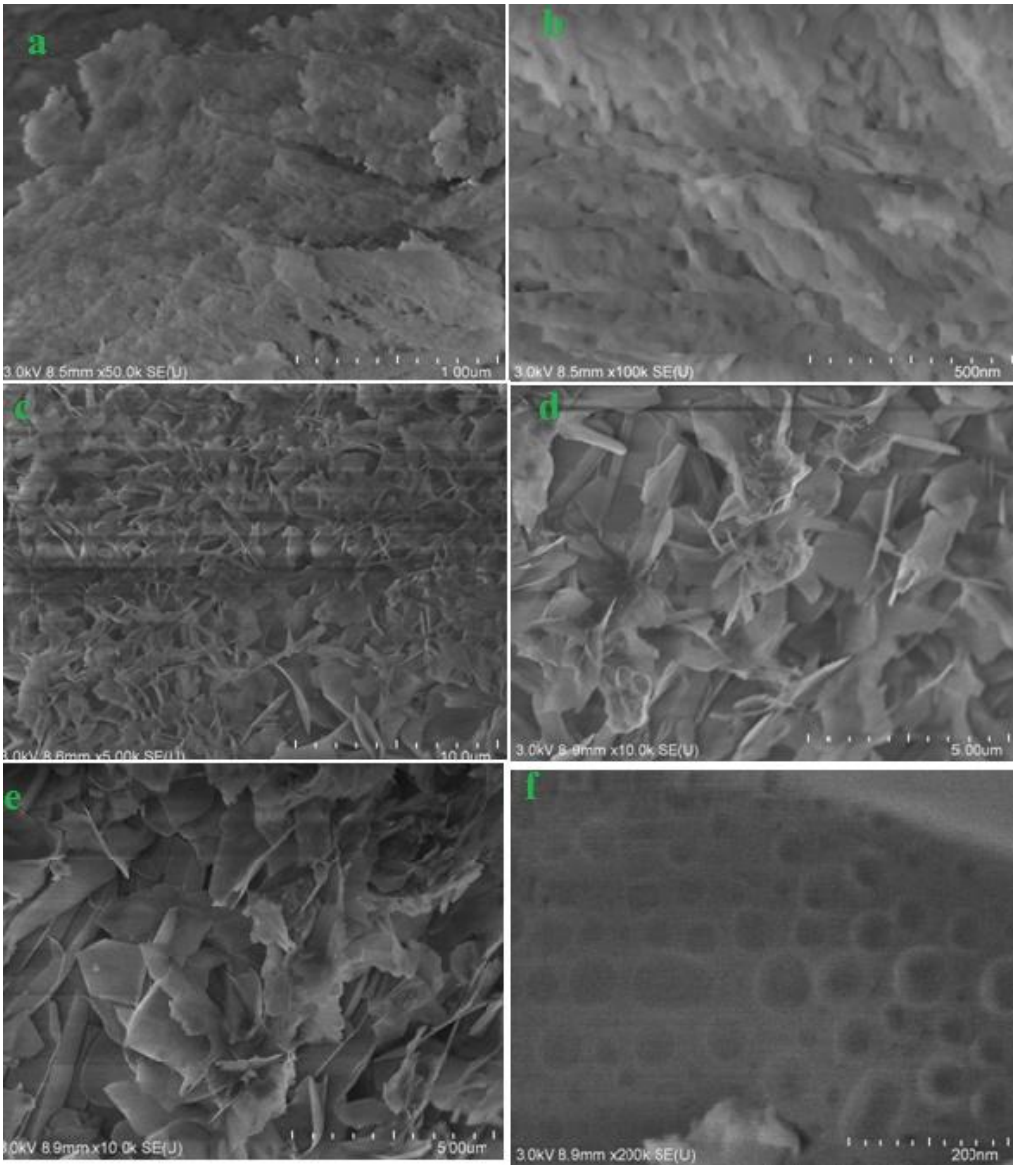

Figure 4.3: FESEM of HA calcined at (a) 600ºC with magnification 50K (b) 600ºC with magnification 100K (c) 800ºC with magnification 5K (d) 800ºC with magnification 10K (e) 1100ºC with magnification 10K (f) 1100ºC with magnification 200K

The hydroxyapatite powders demonstrated diversified propensity to agglomeration. The sample calcined at 1100ºC show grain growth, closely packed particles, rod like structure as well as decreasing pore sizes and density. In addition, the micrographs show morphologies for all samples with fine particles and reduced pore size details (magnification 10.0 K). With an increase to 200.0 K, it is observed that the particles are clustered with more pore size details revealed. The pore size ranges from 31.3 nm to 101 nm provides good agreement to be used in a biomedical application.

The morphology of the HA produced from bone ash might be influenced by the type of animal, the age of the animal and also the type of nutrition of that particular animal from which the bone for this study was obtained [25]. Unfortunately, there was no control on the age and nutrition of the calves from which the bone was obtained. Thus, further study is necessary to look at the influence of these biological factors on the morphology of HA. When bone is heated gradually from 600^{o}C to 1100^{o}C, color changes and also micro structural changes occur which include re-crystallization of the bone mineral. Changes in color, morphology and also re-crystallization of bone minerals due to heating [25][60]. The images of all the samples showed a good homogeneity. The homogeneity was rather found better with good pore structure. This can be found suitable for tissue in-growth. Therefore, based on the results reported here, it can be inferred that the HA can be exploited for producing materials for bone replacement purposes.

4.1.4 Energy Dispersive X-Ray (EDX) Analysis

The highly pronounced Ca and P peaks indicate that the material exhibits a similar framework as standard HA [60]. Based on the chemical structure of standard HA, the Ca/P stoichiometric ratio is approximately 1.67 [60][61][29]. The EDX analysis of HA prepared at 600°C, 800°C and 1100°C showed that Calcium and Phosphorous are the major constituent of bone. This shows that the Ca/P ratio of HA varies between 1.67 to 1.70 which fall within the acceptable range of 1.4–2.4 for atomic Ca/P ratio of stable HA[29][25]. Therefore, the value obtained here is reasonably acceptable and since it is in close agreement with the stoichiometric ratio of normal apatite, it can be regarded as a bone-like apatite[62].

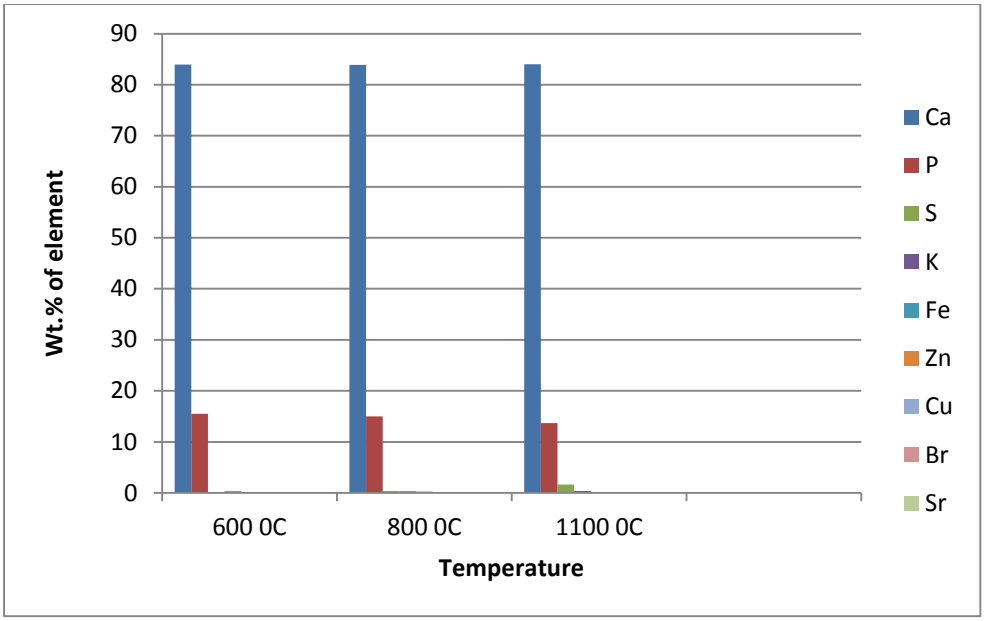

Figure 4.4: Wt. % of different element present at 600ºC, 800ºCand 1100ºC.

It was also found that the wt% of Ca in the HA was slightly increased due to the removal of other organic impurities present in the bone. On other hand wt% of P in the HA is slightly decreased due the loss of Phosphorous in their oxide form after calcinations [29][61].

The little variation in this value is due to the presence of a trace amount of CO_3^{-2} ions as confirmed by FTIR result. The results revealed a large amount of calcium and phosphorus whereas other minor elements existed in lesser amounts. It is interesting to note that aside from calcium, phosphorus, and oxygen, six other elements were detected in HA. It is not surprising to find large amounts of calcium and phosphorus knowing well that these are the main elemental components of HA. Oxygen is also well expected in reasonable amounts since it is a component of phosphate and carbonate. Calcified tissues contain CO_3^{-2} in total of about 3–6 wt% and its presence in HA is of high benefit. Carbon is a component of carbonate and its reasonable amount present in the HA indicates the substitution of carbonates into the HA structure as confirmed through FTIR result. Interestingly, the presence of a reasonable proportion of CO_3^{-2} and other minor elements is desirable for good biological activities of HA, making HA to produced a suitable candidate for bone replacement purposes [60][29][25].

4.2 Characterization of composite

4.2.1 X-Ray Diffraction (XRD) analysis

XRD patterns of the pure PBAT and PBAT/HA nano-composite is shown in figure 4.5. Some reflections appeared in the XRD pattern of pure PBAT at 2θ:18.55°, 21.77°. 24.90° and 26.64°, which indicate the crystalline structure of PBAT [38][66]. The maximum main reflection at 2θ: 24.90° is attributed to (200) planes of orthorhombic crystalline structure of PBAT [67][68]. The broad peaks at 26.64° present in pure PBAT is disappear in HA/PBAT composites, which may be due to the combined effect of HA and PBAT in the composite [69].

In the XRD patterns of PBAT containing HA, the reflections related to HA are not clearly observed due to its lower content, which indicates the effective presence of organic modifier and consequently the better dispersion [68][38]. But high content of HA nano-particles can led to agglomeration area in the PBAT matrix and appearing reflections related to HA nano-particles. The possible reason for poor crystallinity of precipitated HA may be the size effect owing to the three-dimensional network microstructure provided by PBAT in which growth of HA is limited [68].

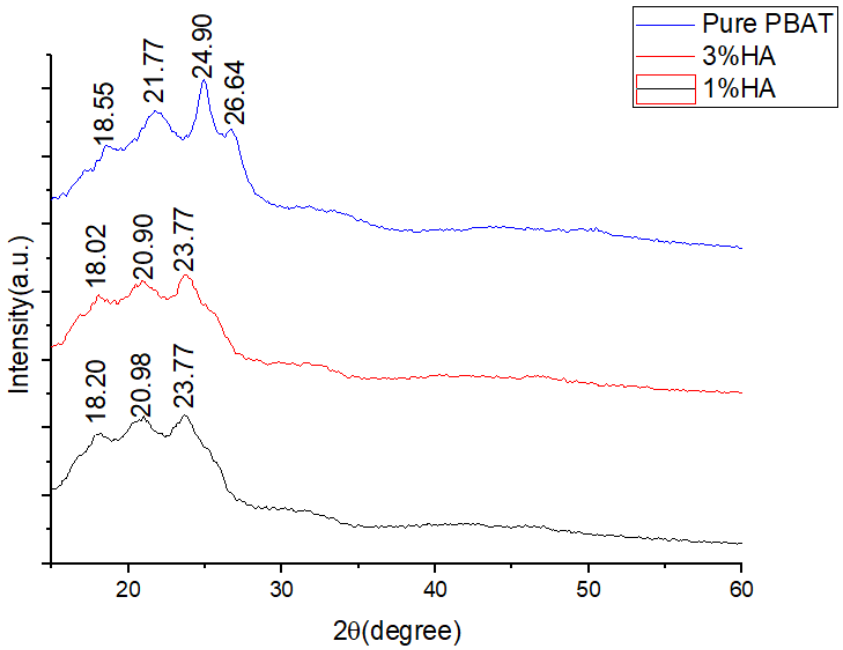

Figure 4.5: XRD pattern of pure PBAT and 1% and 3% HA/PBAT nanocomposite

4.2.2 Fourier Transform Infrared (FTIR) Analysis

The main IR peaks of PBAT are 2958 cm^{-1}, 2875 cm^{-1}, 1392 cm^{-1}, 1366 cm^{-1}, 1169 cm^{-1}, 1121 cm^{-1}, and 937 cm^{-1}. The appearance of 1121 cm^{-1} and 937 cm^{-1} will help to identify PBAT [70][71] . More specifically, the peak assigned at 3065 cm^{-1} in PBAT due to the ¼C-H absorbance in stretching mode [70][5][72]; 2970 cm^{-1}, 2909 cm^{-1} to CH_3-CH_2 stretching mode in aliphatic and aromatic portions [70][73][13]; 1615 cm^{-1}, 1579 cm^{-1}, 1504 cm^{-1} to skeleton vibration of benzene ring [70][13]; 1409 cm^{-1} to bending mode of O-CH_2 [13][72]; 1340 cm^{-1} to out-plane bending mode of CH_2 [72]; at around 1710 cm^{-1} representing carbonyl groups (C=O) in the ester linkage (i.e. for the stretching vibration of the –COO–) [74][5][13][72][70]; 1254 cm^{-1}, 1105 cm^{-1} to C-O stretching mode in the ester linkage (i.e. for the stretching vibration of the C-O-C) [74][13][72]; 1020 cm^{-1} to in-plane bending mode of ¼C-H in benzene ring [72][70]; and 974 $cm^{-1}$to C-O stretching mode.

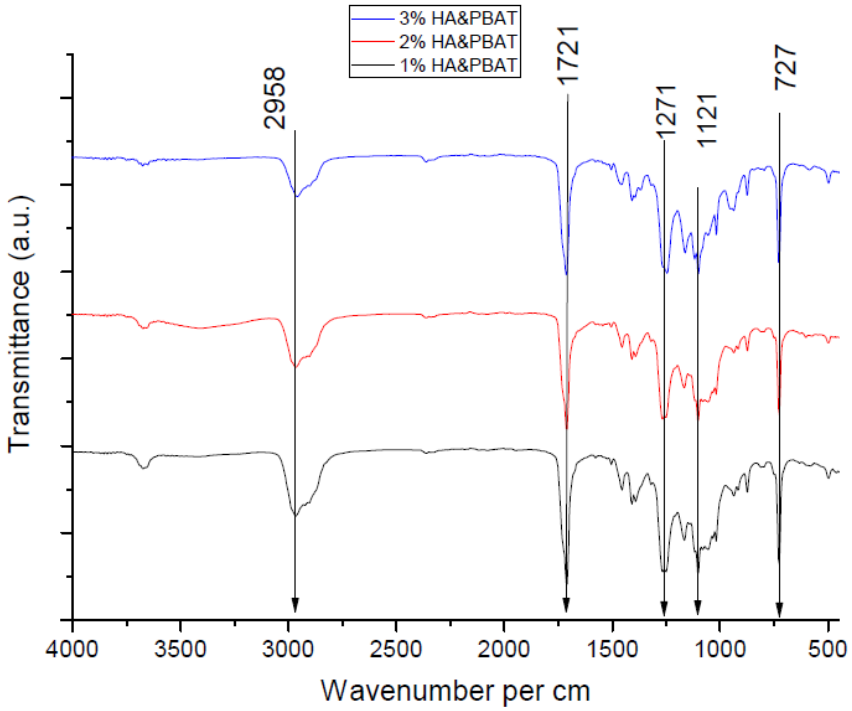

Figure 4.6: FTIR spectra of pure PBAT and PBAT/HA nano-composite

The peak assigned at 875 $cm^{-1}$and 731 cm^{-1} is out-plane bending mode of ¼C-H in benzene ring and 850 cm^{-1} is in-plane bending mode of CH_2 [70][6][75]. The absorbance at 1339 cm^{-1}, 972 cm^{-1}, and 849 cm^{-1} increased with increase in crystallinity of HA. The out-plane bending mode of ¼C-H in benzene ring

generally appeared in 830 cm^{-1}, but influenced by the conjugation of C=O and the benzene ring, the absorbance occurred in 730 cm^{-1} [72]. Peak at 1121 $cm^{-1}$and 1169 cm^{-1} should be assigned as the stretching mode of the C-O in alphabetic acid [70]. Bending peaks of the benzene substitutes are located at wave numbers between 700 and 900 cm^{-1} [74].

Table 4.3: Different functional group present on composite

Wave numbers (cm^{-1})	**Chemical Bonding**	**Vibration**
3065, 2819	=C-H	stretching mode
2958	CH_2	asymmetric Stretching mode
2875	CH_2	symmetric stretching mode
1721, 1710	C=O	stretching mode
1578, 1504	Benzene ring	skeleton vibration
1457	CH_2	CH_2 in plane bending mode
1271, 1105	C-O connected to benzene rings	stretching mode
1019	=C-H in benzene ring	in plane bending mode
875, 731	=C-H in benzene ring	out plane bending mode
1121, 1169	C-O in alphabetic acid	stretching mode
1336-1522	C=O in phenolic group	stretching mode
700-900	Benzene substitute	stretching mode
727	$CH_2$of benzene	deformation mode

The deposition of HA in PBAT can be confirmed by FTIR. The peak which is not seen in pure HA (at around 3600 $cm^{-1)}$ which is visible in PBAT/HA composite may be due to the combined effect of HA and PBAT in the composite. Peak of HA and PBAT both are appeared in the FTIR spectra of composite clearly indicates homogeneous distribution of HA in the composite. With the increase in percentage of HA in PBAT, more clear and narrower peak of OH^-group at 3600$cm^{-1}$and more clear peak of PO_4 group at around 1100 $cm^{-1}$are shown. Therefore, based on the results reported herein, it can be inferred that the composite of HA and PBAT can be exploited for producing filament of 3D printing.

4.3 Assessment of Biodegradability

4.3.1 Water Absorption Test

The composite of 1%, 2% and 3% HA/PBAT and pure PBAT were immersed in water at room temperature. They were then taken out at specific time intervals and gently blotted with paper towel to remove surface excess water before weighing. The percentage of water absorbed was calculated using the formula below [76]:

$$\%\ of\ water\ absorbed\ = \frac{M_x - M_o}{M_o} \times 100\%$$

Where, Mx and Mo indicate the weights of the collected sample and the initial weight of the sample respectively.

The water uptake in polymer may affect its mechanical properties, degradability, and dimensional stability. Water exposure and uptake may decrease the life of a polymer due to hydrolysis and micro crack formation. The percentages of water absorption for PBAT/HA composite are shown in Table 4.2.

Table 4.4: Percentage of water absorbed for HA/PBAT composite with various amount of HA

	Wt. gain % in 1 days	**Wt. gain % in 3 days**	**Wt. gain % in 7 days**	**Wt. gain % in 15 days**
Pure PBAT	0.23	1.37	3.01	3.25
1.5% HA/PBAT	0.45	1.45	3.22	3.45
2% HA/PBAT	0.62	2.12	3.78	3.98
3% HA/PBAT	0.92	2.56	4.13	4.23

The weight gained percentage of pure PBAT is 3.25% after 15 days. Since PBAT is hydrophilic (containing more polar group) in nature which provides the site to form hydrogen bond with water. Greater the hydrophilicity, greater will be the water absorption property. This also might be attributed to the swelling of the PBAT when it is exposed to water which leads to crack formation. Micro-cracks can produce pathways for easier diffusion of the water molecules into the composite and thus improve their water absorption [72]. That's why PBAT gained weight after it is exposed to the water. The pure PBAT

show the lowest percentage of weight gained and 3% HA/PBAT show the highest percentage of weight gained. As the percentage of HA is increased, the percentage of water absorption increases. The weight gained percentage of 3% HA/PBAT was found to be 4.23% after 15 days. The surface of the hydroxyapatite has a "liquid-loving" property, which may be due to the nature of chemical bonding present in hydroxyapatite [48]. It contain hydroxyl group which provides the site for the hydrogen bond with water. Additionally, the flexible and highly interconnected porous structure HA provided most rapid water access. Highly porous HA also had high water uptake ratio [9]. HA contain pore with nanometer size as conformed by SEM image and this provides the site for the water absorption [48].

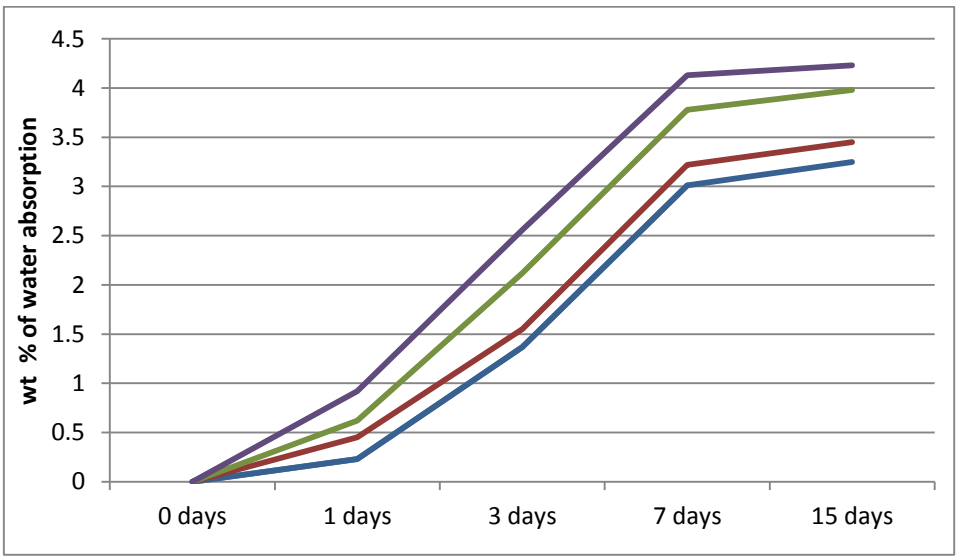

Figure 4.7: Plot of days Vs water absorption by composite

So, there is a synergetic effect of hydrophilic nature of PBAT and also hydrophilic nature of HA provides the good site for the water absorption. That's why with increased the percentage of HA in composite, water absorption property increased and also weight gain increased.

4.3.2 Tris-Buffer Test

Biodegradibility of the samples were tested in 0.5 M tris-buffer solution. First, dry weight of the 0%, 1%, 2% and 3% HA/PBAT filament was taken. Then it is dipped into this buffer solution and kept in incubator at 37°C and pH is

maintained at 7.4. The samples are then taken out in 1 day, 3days, 7 days, 15 days and 30 days, washed with distilled water and were dried and then dry weight taken. The percentage weight reduction was calculated [77]. PBAT undergoes hydrolytic degradation owing to the cleavage of ester linkages, which requires the presence of water. However, H_2O can even react with the carbonyl groups located in proximity of benzene rings (subpanel b). β-C-H hydrogen transfer reactions are supposed to occur randomly even in PBAT backbone[78]. The degradation determines a dramatic molecular weight reduction and can be easily monitored by spectroscopic measurement of –OH and –COOH groups[78].

The percentage weight loss was calculated using the formula below:

$$\%\, of\ weight\ loss\ = \frac{W_x - W_o}{W_o} \times 100\%$$

where, Wx and Wo indicate the weights of the collected sample and the initial weight of the sample respectively.

After dipping into the tris buffer solution for 30 days, the results came positive. There was a 6.21% decrease in pure PBAT, a 6.11% decrease in 1.5% HA/PBAT, a 6.01% decrease in 2% HA/PBAT and a 5.99% decrease 3% HA/PBAT. It was found that wt. loss percentage gone to decrease with increased percentage of HA in composite and highest reduction percentage is found in pure PBAT. This is because in composite only PBAT is degradable and HA is non degradable.

Table 4.5: Percentage of degradation for HA/PBAT composite with various amount of HA

	Wt. loss % in 1st days	**Wt. loss % in 3rd days**	**Wt. loss % in 7th days**	**Wt. loss % in 15th days**	**Wt. loss % in 30th days**
0% HA/PBAT	0	0	0.25	3.13	6.21
1.5% HA/PBAT	0	0	0.15	3.01	6.11
2% HA/PBAT	0	0	0.15	2.99	6.01
3% HA/PBAT	0	0	0.098	2.92	5.99

With the increased in percentage of HA, the non degradable part increased in the composite and degradable part is decreased. Many researcher claims that that degradation percentage was gone to increased after 8 weeks [78][77].

Above result conform that if composite is used in a bone regeneration application, the PBAT is full degraded after certain month but HA remain unchanged. With increase the percentage of HA, the degradation rate decreased. This is because only PBAT is biodegradable and HA is not degradable. This can be found suitable for tissue in growth. Therefore, based on the results reported here, it can be inferred that the HA can be exploited for producing materials for bone replacement purposes.

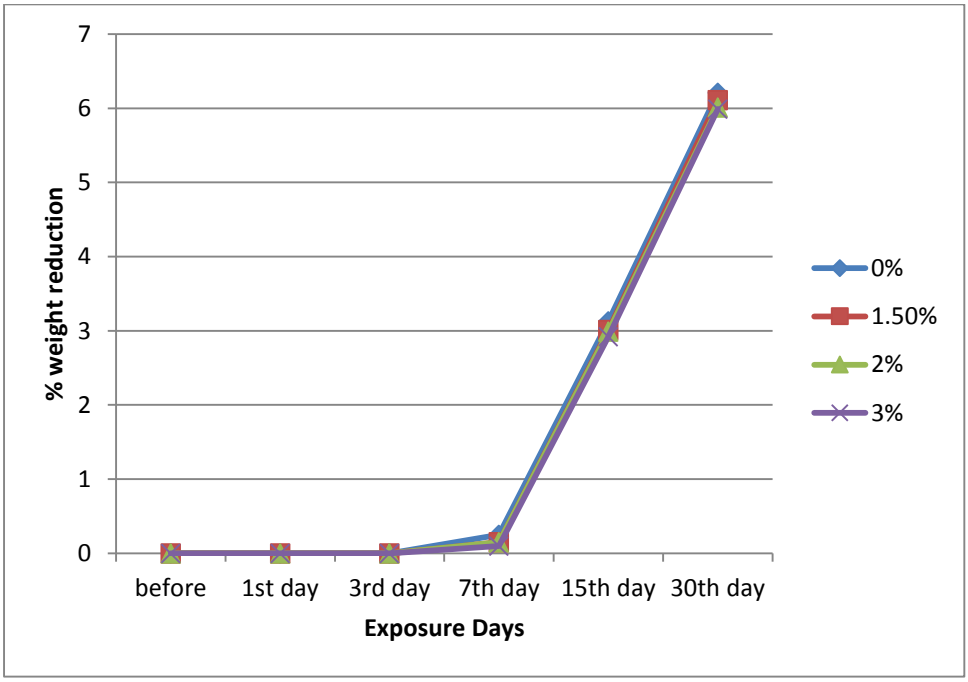

Figure 4.8 Plot of days Vs weight reduction percentage of composite

4.4 Biological Activity

For the antimicrobial test, first we have to prepare NHA media plate. This media plate was incubate for 24 hour at 37^{o}C so that the clear zone was seen and media plate does not contain any contamination. Then, media plate was divided into two half and with the help of loop, moss was cultured in the plate. The plate is again incubate for 15 minute. For the qualitative measurement of antimicrobial activity, a small piece of film samples were punched to make disks and the antimicrobial activity was determined using a modified agar diffusion assay and

it was again incubate for 24 hours. An inhibition zone tested the antimicrobial activity of PBAT and PBAT/HA nano-composite films. The *Escherichia coli* bacteria was used for finding the antimicrobial activity of the films[73].

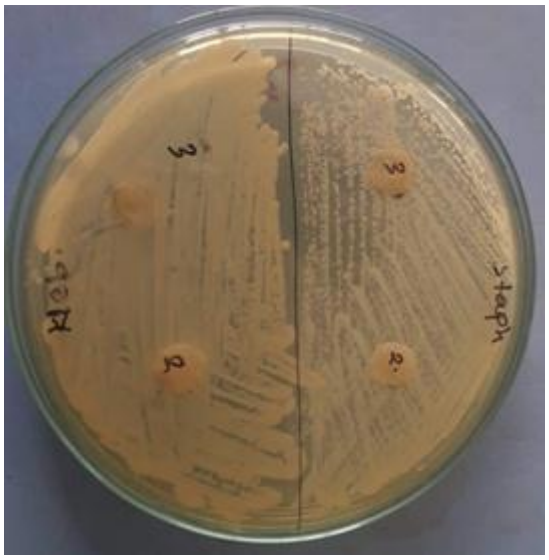

Figure 4.9: Antimicrobial test of HA/PBAT composite (a) 3 means 3% HA/PBAT composite film (b) 1.5% HA/PBAT composite film.

As many researcher claims that PBAT films do not show clear microbial inhibition zones. HA incorporated PBAT nano-composite films also do not exhibit distinctive microbial inhibition zones for both the microorganisms. This indicates that HA nano-particles do not exhibit fair antimicrobial action against *E. coli.* Both films do not show any antimicrobial test. If we want to make composite antimicrobial, we have to add third substance like Ag_2O[73], Boron[9] which show antimicrobial test so that composite also shows antimicrobial test.

CHAPTER 5: CONCLUSION AND RECOMMENDATION

5.1 Conclusion

The product obtained by the calcinations of bone at the temperature of 600^{o}C, 800^{o}C and 1100^{o}C confirmed that it is possible to obtain hydroxyapatite by thermal treatment of bone waste. The formation of hydroxyapatite nano-particles was confirmed by XRD and FTIR analysis. The elemental compositions were examined by using the EDX analysis. The size and morphology of the samples were characterized by using SEM analysis. The small rod shaped particles was confirmed through the SEM analysis. The particle size of the nano-HA is 40.89 nm at 1100^{o}C was determined by using XRD analysis, which is good agreement with the SEM analysis.

Hydroxyapatite obtained from animal bones can potentially be used as a biomaterial for both surgical and stomatological implants. HA may be applied in orthopaedics, orthognathicsurgery, ophthalmology, laryngology and traumutology. The composite structures of PBAT and HA were successfully produced by solvent casting method. The homogeneous distribution of HA among PBAT was confirmed by FTIR analysis. The results are generally positive, indicating the suitability of the polymer composite for 3D printing directly from pellet forms. The addition of HA brought improvements in hardness of PBAT, due to high interactions between the carbonyl groups of the polymer matrix and the hydroxyl groups of HA. As the percentage of HA is increased, the percentage of water absorption increases. The weight gained percentage of 3% HA/PBAT was found to be 4.23% after 16 days. The surface of the hydroxyapatite has a “liquid-loving” property, which may be due to the nature of chemical bonding present in hydroxyapatite. Since PBAT is hydrophilic (containing more polar group) in nature which provides the site to form hydrogen bond with water. Greater the hydrophilicity, greater will be the water absoption property. Also, it was found that wt. loss percentage gone to decrease with increased percentage of HA in composite and highest reduction percentage is found in pure PBAT. However, further biocompatibility tests should be carried out in order to verify the possible use of these materials for

tissue engineering applications. Therefore, this biomaterial has great potential for applications in regenerative medicine as a support for bone growth.

5.2 Recommendation

The result provides a good background to go the next step and collect a more information about the characteristic, different physical properties, size and mechanical properties of HA. Further, physical properties (such as lattice parameter, particle size, crystallinity and density), mechanical properties (such as tensile strength, youngs modulus, fracture toughness) and thermal stability of HA also evaluated. Particle size and morphology character was characterized by TEM (Tunneling Electron Microscope) and determination of composition of HA in their calcified tissue by XRF (X-Ray Flourescence).

The above discussion enables us to conclude that many studies about PBAT and its composites have been developed, however, there is a need for more studies to make this polymer competitive, therefore expanding their use for more applications. PBAT has the potential to bring significant economic effect in various technology based industrial sectors. Also, we need in-vitro and in-vivo compatibility test of 3D printed sample, tensile strength of composite, TEM and SEM analysis of sample and other mechanical and biocompatibility test of the sample should be carried out in order to verify the possible use of these materials for tissue engineering applications.

REFERENCES

[1] G. Chakraborty, R. B. Valapa, G. Pugazhenthi, and V. Katiyar, "Investigating the properties of poly (lactic acid)/exfoliated graphene based nanocomposites fabricated by versatile coating approach," *Int. J. Biol. Macromol.*, vol. 113, no. 2017, pp. 1080–1091, 2018, doi: 10.1016/j.ijbiomac.2018.03.037.

[2] J. Stagner, "Methane generation from anaerobic digestion of biodegradable plastics – a review," *Int. J. Environ. Stud.*, vol. 73, no. 3, pp. 462–468, 2016, doi: 10.1080/00207233.2015.1108607.

[3] F. V. Ferreira, L. S. Cividanes, R. F. Gouveia, and L. M. F. Lona, "An overview on properties and applications of poly(butylene adipate-co-terephthalate)–PBAT based composites," *Polym. Eng. Sci.*, vol. 59, no. s2, pp. E7–E15, 2019, doi: 10.1002/pen.24770.

[4] V. R. Feig, H. Tran, and Z. Bao, "Biodegradable polymeric materials in degradable electronic devices," *ACS Cent. Sci.*, vol. 4, no. 3, pp. 337–348, 2018, doi: 10.1021/acscentsci.7b00595.

[5] Z. N. Correa-Pacheco *et al.*, "Preparation and characterization of bio-based PLA/PBAT and cinnamon essential oil polymer fibers and life-cycle assessment from hydrolytic degradation," *Polymers (Basel).*, vol. 12, no. 1, pp. 1–32, 2020, doi: 10.3390/polym12010038.

[6] K. Fukushima, M. H. Wu, S. Bocchini, A. Rasyida, and M. C. Yang, "PBAT based nanocomposites for medical and industrial applications," *Mater. Sci. Eng. C*, vol. 32, no. 6, pp. 1331–1351, 2012, doi: 10.1016/j.msec.2012.04.005.

[7] M. Yang, J. Hu, N. Xiong, B. Xu, Y. Weng, and Y. Liu, "Preparation and properties of PLA/PHBV/PBAT blends 3D printing filament," *Mater. Res. Express*, vol. 6, no. 6, 2019, doi: 10.1088/2053-1591/ab06cf.

[8] S. Singamneni, D. Smith, M. J. LeGuen, and D. Truong, "Extrusion 3D printing of polybutyrate-adipate-terephthalate-polymer composites in

the pellet form," *Polymers (Basel).*, vol. 10, no. 8, 2018, doi: 10.3390/polym10080922.

[9] A. Arslan, S. Çakmak, and M. Gümüşderelioğlu, "Enhanced osteogenic activity with boron-doped nanohydroxyapatite-loaded poly(butylene adipate-co-terephthalate) fibrous 3D matrix," *Artif. Cells, Nanomedicine Biotechnol.*, vol. 46, no. sup2, pp. 790–799, 2018, doi: 10.1080/21691401.2018.1470522.

[10] W. Prasong, P. Muanchan, A. Ishigami, S. Thumsorn, T. Kurose, and H. Ito, "Properties of 3D printable Poly(lactic acid)/Poly(butylene adipate-co-terephthalate) Blends and Nano Talc Composites," *J. Nanomater.*, vol. 2020, 2020, doi: 10.1155/2020/8040517.

[11] Q. Yao, Z. Song, J. Li, and L. Zhang, "Micromorphology, mechanical, crystallization and permeability properties analysis of HA/PBAT/PLA (HA, hydroxyapatite; PBAT, poly(butylene adipate-co-butylene terephthalate); PLA, polylactide) degradability packaging films," *Polym. Int.*, vol. 69, no. 3, pp. 301–307, 2020, doi: 10.1002/pi.5953.

[12] A. F. Jaramillo *et al.*, "Comparative study of the antimicrobial effect of nanocomposites and composite based on Poly(butylene adipate-co-terephthalate) using Cu and Cu/Cu2O nanoparticles and CuSO4," *Nanoscale Res. Lett.*, vol. 14, 2019, doi: 10.1186/s11671-019-2987-x.

[13] D. Maria *et al.*, "In Vivo evaluation of the genotoxic effects of poly nanohydroxyapatite scaffolds for bone regeneration," pp. 1–16.

[14] W. A. Ribeiro Neto *et al.*, "Poly (butylene adipate-co-terephthalate)/hydroxyapatite composite structures for bone tissue recovery," *Polym. Degrad. Stab.*, vol. 120, pp. 61–69, 2015, doi: 10.1016/j.polymdegradstab.2015.06.009.

[15] L. R.Z. and D. G.D., "Musculoskeletal tissue regeneration. In S.P. William(Eds)," *Biol. Mater. Methods*, p. 153, 2008.

[16] B. Viswanath and N. Ravishankar, "Controlled synthesis of plate-shaped hydroxyapatite and implications for the morphology of the apatite phase

in bone," *Biomaterials*, vol. 29, no. 36, pp. 4855–4863, 2008, doi: 10.1016/j.biomaterials.2008.09.001.

[17] S. V. Dorozhkin, "Bioceramics of calcium orthophosphates," *Biomaterials*, vol. 31, no. 7, pp. 1465–1485, 2010, doi: 10.1016/j.biomaterials.2009.11.050.

[18] E. M. Rivera-muñoz, "Hydroxyapatite-Based Materials : Synthesis and characterization," 2000.

[19] V. P. Orlovskii, V. S. Komlev, and S. M. Barinov, "Hydroxyapatite and hydroxyapatite-based ceramics," *Inorg. Mater.*, vol. 38, no. 10, pp. 973–984, 2002, doi: 10.1023/A:1020585800572.

[20] S. S and C. P, "Improvement of mechanical properties of 3d printed hydroxyapatite scaffolds by polymeric infiltration," *Bioceram. Dev. Appl.*, vol. 3, no. s1, pp. 10–12, 2013, doi: 10.4172/2090-5025.s1-012.

[21] J. Venugopal, M. P. Prabhakaran, Y. Zhang, S. Low, A. T. Choon, and S. Ramakrishna, "Biomimetic hydroxyapatite containing composite nanofibrous substrates for bone tissue engineering," *Philos. Trans. R. Soc. A Math. Phys. Eng. Sci.*, vol. 368, no. 1917, pp. 2065–2081, 2010, doi: 10.1098/rsta.2010.0012.

[22] R. Saidi, M. H. Fathi, and H. Salimijazi, "Fabrication and characterization of hydroxyapatite-coated forsterite scaffold for tissue regeneration applications," *Bull. Mater. Sci.*, vol. 38, no. 5, pp. 1367–1374, 2015, doi: 10.1007/s12034-015-1022-9.

[23] L. Sopyan, R. Singh, and M. Abd Shukor, "Syntheisi of nano sized hydroxyapatite powder using sol-gel technique and its consersion to dense and porous bodies," *Indian J. Chmeistry-Section A Inorganic, Phys. Thereotical Anal. Chem.*, vol. 47, pp. 1626–1631, 2008.

[24] K. Horie *et al.*, "Definitions of terms relating to reactions of polymers and to functional polymeric materials: (IUPAC Recommendations 2003)," *Pure Appl. Chem.*, vol. 76, no. 4, pp. 889–906, 2004, doi: 10.1351/pac200476040889.

[25] F. A. Zakaria, “Sintering and microstructure property relationships of porous hydroxyapatite,” p. 202, 2000, [Online]. Available: http://search.proquest.com/docview/1466288370?accountid=45159.

[26] C. R. Bhatta, “Synthesis of hydroxyapatite from egg shell and to incorporate it into resorcinol formaldehyde resin. Trichandra multiple campus, A project report submitted to Department of Chemistry, Trichandra Multiple Campus, Tribhuvan University,” 2016.

[27] D. N. de Planeación, “Hydroxyapatite and its characterization, vol. 66, pp. 37–39, 2012, [Online]. Available: https://www.boe.es/buscar/pdf/2003/BOE-A-2003-20838-consolidado.pdf.

[28] R. Z. LeGeros, *Calcium phosphates in oral biology and medicine*, 15th ed. new work: Monographs in oral science, 1991.

[29] L. L. Hench, J. Wilson, R. Z. LeGeros, and J. P. LeGeros, “Dense Hydroxyapatite,” *An introd. to bioceram.*, pp. 139–180, 1993, doi: 10.1142/9789814317351_0009.

[30] F. Chen, Z. C. Wang, and C. J. Lin, “Preparation and characterization of nano-sized hydroxyapatite particles and hydroxyapatite/chitosan nano-composite for use in biomedical materials,” *Mater. Lett.*, vol. 57, no. 4, pp. 858–861, 2002, doi: 10.1016/S0167-577X(02)00885-6.

[31] W. Zhu, X. Ma, M. Gou, D. Mei, K. Zhang, and S. Chen, “3D printing of functional biomaterials for tissue engineering,” *Curr. Opin. Biotechnol.*, vol. 40, pp. 103–112, 2016, doi: 10.1016/j.copbio.2016.03.014.

[32] A. Aimar, A. Palermo, and B. Innocenti, “The role of 3D printing in medical applications: A State of the Art,” *J. Healthc. Eng.*, vol. 2019, 2019, doi: 10.1155/2019/5340616.

[33] A. Pandian and C. Belavek, “A review of recent trends and challenges in 3D printing,” *Proc. 2016 ASEE North Cent. Sect. Conf.*, pp. 1–17, 2017.

[34] M. C. Piazza and S. E. Alexander, “Additive manufacturing: a summary of the literature,” *Coll. Urban Aff.*, 30, 2015, [Online]. Available: http://urban.csuohio.edu.

[35] I. V. Zlobina, N. V. Bekrenev, and S. P. Pavlov, “A proposal to improve a 3D printing technology of composite materials products,” *IOP Conf. Ser. Mater. Sci. Eng.*, vol. 286, no. 1, 2018, doi: 10.1088/1757-899X/286/1/012017.

[36] R. Matsuzaki *et al.*, “Three-dimensional printing of continuous-fiber composites by in-nozzle impregnation,” *Sci. Rep.*, vol. 6, no. February, pp. 1–7, 2016, doi: 10.1038/srep23058.

[37] V. Malkoc, “Challenges and the future of 3D bioprinting.,” *J. Biomed. Imaging Bioeng.*, vol. 1, no. 3, pp. 62–63, 2018.

[38] J. Obielodan, J. Helman, and A. Grumbles, “Development of a thermoplastic biocomposite for 3D printing,” *Solid Free. Fabr. 2018 Proc. 29th Annu. Int. Solid Free. Fabr. Symp. - An Addit. Manuf. Conf. SFF 2018*, pp. 847–852, 2020.

[39] B. Tisserat, Z. Liu, V. Finkenstadt, B. Lewandowski, S. Ott, and L. Reifschneider, “3D printing biocomposites,” *SPE Plast. Res. Online*, pp. 10–12, 2015.

[40] C. E. Corcione *et al.*, “3D printing of hydroxyapatite polymer-based composites for bone tissue engineering,” *J. Polym. Eng.*, vol. 37, no. 8, pp. 741–746, 2017, doi: 10.1515/polyeng-2016-0194.

[41] C. A. Beevers and D. B. McIntyre, “The atomic structure of fluor-apatite and its relation to that of tooth and bone material. (With Plates XVI-XVIII.),” *Mineral. Mag. J. Mineral. Soc.*, vol. 27, no. 194, pp. 254–257, 1946, doi: 10.1180/minmag.1946.027.194.05.

[42] L. Calderín, M. J. Stott, and A. Rubio, “Electronic and crystallographic structure of apatites,” *Phys. Rev. B - Condens. Matter Mater. Phys.*, vol. 67, no. 13, pp. 1–7, 2003, doi: 10.1103/PhysRevB.67.134106.

[43] B. N. Johnson *et al.*, "3D Printed Anatomical Nerve Regeneration Pathways," *Adv. Funct. Mater.*, vol. 25, no. 39, pp. 6205–6217, 2015, doi: 10.1002/adfm.201501760.

[44] R. Lozano *et al.*, "3D printing of layered brain-like structures using peptide modified gellan gum substrates," *Biomaterials*, vol. 67, pp. 264–273, 2015, doi: 10.1016/j.biomaterials.2015.07.022.

[45] C. N. Ludvik, G. M. Glenn, A. P. Klamczynski, and D. F. Wood, "Cellulose fiber/bentonite clay/biodegradable thermoplastic composites," *J. Polym. Environ.*, vol. 15, no. 4, pp. 251–257, 2007, doi: 10.1007/s10924-007-0072-5.

[46] Z. Yang, H. Peng, W. Wang, and T. Liu, "Crystallization behavior of poly(ε-caprolactone)/layered double hydroxide nanocomposites," *J. Appl. Polym. Sci.*, vol. 116, no. 5, pp. 2658–2667, 2010, doi: 10.1002/app.

[47] M. Dressler *et al.*, "Influence of gelatin coatings on compressive strength of porous hydroxyapatite ceramics," *J. Eur. Ceram. Soc.*, vol. 31, no. 4, pp. 523–529, 2011, doi: 10.1016/j.jeurceramsoc.2010.11.004.

[48] J. K. Odusote, Y. Danyuo, A. D. Baruwa, and A. A. Azeez, "Synthesis and characterization of hydroxyapatite from bovine bone for production of dental implants," *J. Appl. Biomater. Funct. Mater.*, vol. 17, no. 2, 2019, doi: 10.1177/2280800019836829.

[49] H. Gheisari and E. Karamian, "Preparation and characterization of hydroxyapatite reinforced with hardystonite as a novel bio-nanocomposite for tissue engineering," vol. 19, no. 5, pp. 141–152, 2015, [Online]. Available: http://nmj.mums.ac.ir.

[50] R. D. Panggabean and Y. Yusuf, "Preparation and characterization of hydroxyapatite based on human teeth with various of calcination," *Proc. - 2018 1st Int. Conf. Bioinformatics, Biotechnol. Biomed. Eng. BioMIC 2018*, vol. 1, pp. 1–4, 2019, doi: 10.1109/BIOMIC.2018.8610554.

[51] E. Kusrini, A. R. Pudjiastuti, S. Astuningsih, and S. Harjanto,

"Preparation of hydroxyapatite from bovine bone by combination methods of ultrasonic and spray drying," *Int. Conf. Chem. Bio-Chemical Environ. Sci.*, pp. 47–51, 2012.

[52] J. Venkatesan and S. K. Kim, "Effect of temperature on isolation and characterization of hydroxyapatite from tuna (thunnus obesus) bone," *Materials (Basel).*, vol. 3, no. 10, pp. 4761–4772, 2010, doi: 10.3390/ma3104761.

[53] S. Mondal, B. Mondal, A. Dey, and S. S. Mukhopadhyay, "Studies on processing and characterization of hydroxyapatite biomaterials from different bio wastes," *J. Miner. Mater. Charact. Eng.*, vol. 11, no. 01, pp. 55–67, 2012, doi: 10.4236/jmmce.2012.111005.

[54] A. Sobczak-Kupiec, D. Malina, R. Kijkowska, and Z. Wzorek, "Comparative study of hydroxyapatite prepared by the authors with selected commercially available ceramics," *Dig. J. Nanomater. Biostructures*, vol. 7, no. 1, pp. 385–391, 2012.

[55] M. S. E. A. G. and M. I. N. I. J.Juraida, "Preparation and characterization of hydroxyapatite from fish bone," *Umtas 2011*, p. 76, 2011, [Online]. Available:http://www.umt.edu.my/dokumen/UMTAS2011/CHEM_PHY/Oral_CHEM_PHY/PCO11_M. Sontang.pdf.

[56] G. Gergely *et al.*, "Preparation and characterization of hydroxyapatite from eggshell," *Ceram. Int.*, vol. 36, no. 2, pp. 803–806, 2010, doi: 10.1016/j.ceramint.2009.09.020.

[57] M. E. Bahrololoom, M. Javidi, S. Javadpour, and J. Ma, "Characterisation of natural hydroxyapatite extracted from bovine cortical bone ash," *J. Ceram. Process. Res.*, vol. 10, no. 2, pp. 129–138, 2009.

[58] Y. Luo, W. Li, F. Wang, and J. Zou, "Synthesis and characterization of fluorine-substituted hydroxyapatite powder by polyacrylamide-gel method," *Adv. Mater. Res.*, vol. 152–153, no. 8, pp. 1305–1308, 2011, doi: 10.4028/www.scientific.net/AMR.152-153.1305.

[59] N. R. Parsons, “Novel methods of microwave-assisted and albumen-mediated synthesis of nano-apatites from eggshell and egg white for tissue engineering,” no. April, 2013.

[60] J. O. Akindoyo, S. Ghazali, M. D. H. Beg, and N. Jeyaratnam, “Characterization and elemental quantification of natural hydroxyapatite produced from cow bone,” *Chem. Eng. Technol.*, vol. 42, no. 9, pp. 1805–1815, 2019, doi: 10.1002/ceat.201800636.

[61] J. K. Abifarin, D. O. Obada, E. T. Dauda, and D. Dodoo-Arhin, “Experimental data on the characterization of hydroxyapatite synthesized from biowastes,” *Data Br.*, vol. 26, p. 104485, 2019, doi: 10.1016/j.dib.2019.104485.

[62] M. J. Bailey, S. Coe, D. M. Grant, G. W. Grimea, and C. Jeynes, “Accurate determination of the Ca : P ratio in rough hydroxyapatite samples by SEM-EDS, PIXE and RBS - A comparative study,” *X-Ray Spectrom.*, vol. 38, no. 4, pp. 343–347, 2009, doi: 10.1002/xrs.1171.

[63] K. Wei *et al.*, “Synthesis and characterization of hydroxyapatite nanobelts and nanoparticles,” *Mater. Lett.*, vol. 59, no. 2–3, pp. 220–225, 2005, doi: 10.1016/j.matlet.2004.08.034.

[64] K. Paljar, S. Orlić, E. Tkalčec, and H. Ivanković, “Izvorni znanstveni rad / Original scientific paper,” *Chem. Eng.*, pp. 158–165, 2006.

[65] N. Monmaturapoj, “Nano-size hydroxyapatite powders preparation by wet-chemical precipitation route,” *J. Met. Mater. Miner.*, vol. 18, no. 1, pp. 15–20, 2008.

[66] Y. L. Pak *et al.*, “Layered double hydroxide nanocomposites,” vol. 2013, 2013.

[67] S. Liu *et al.*, “Preparation and characterisation of a lamellar hydroxyapatite/polylactic acid composite,” *Plast. Rubber Compos.*, vol. 48, no. 2, pp. 66–73, 2019, doi: 10.1080/14658011.2018.1548191.

[68] M. Hajibeygi and S. Shafiei-Navid, “Design and preparation of

poly(lactic acid) hydroxyapatite nanocomposites reinforced with phosphorus-based organic additive: Thermal, combustion, and mechanical properties studies," *Polym. Adv. Technol.*, vol. 30, no. 9, pp. 2233–2249, 2019, doi: 10.1002/pat.4652.

[69] J. M. Ferri, J. Jordá, N. Montanes, O. Fenollar, and R. Balart, "Manufacturing and characterization of poly(lactic acid) composites with hydroxyapatite," *J. Thermoplast. Compos. Mater.*, vol. 31, no. 7, pp. 865–881, 2018, doi: 10.1177/0892705717729014.

[70] Y. Cai *et al.*, "Discrimination of poly(butylenes adipate-co-terephthalate) and poly(ethylene terephthalate) with fourier transform infrared microscope and Raman spectroscope," *Spectrosc. Lett.*, vol. 45, no. 4, pp. 280–284, 2012, doi: 10.1080/00387010.2011.610420.

[71] R. Al-itry, "Blends based on poly (lactic acid) : structure / rheology / processing relationship To cite this version : Mélanges de polymères à base de Poly (acide lactique) : Relation Structure / rhéologie / procédés de mise en forme," 2013.

[72] S. Siyamak, N. A. Ibrahim, S. Abdolmohammadi, W. M. Z. Wan Yunus, and M. Z. A. B. Rahman, "Effect of fiber esterification on fundamental properties of oil palm empty fruit bunch fiber/poly(butylene adipate-co-terephthalate) biocomposites," *Int. J. Mol. Sci.*, vol. 13, no. 2, pp. 1327–1346, 2012, doi: 10.3390/ijms13021327.

[73] R. Venkatesan, N. Rajeswari, and A. Tamilselvi, "Antimicrobial, mechanical, barrier, and thermal properties of bio-based poly (butylene adipate-co-terephthalate) (PBAT)/Ag2O nanocomposite films for packaging application," *Polym. Adv. Technol.*, vol. 29, no. 1, pp. 61–68, 2018, doi: 10.1002/pat.4089.

[74] R. Muthuraj, M. Misra, and A. K. Mohanty, "Hydrolytic degradation of biodegradable polyesters under simulated environmental conditions," *J. Appl. Polym. Sci.*, vol. 132, no. 27, 2015, doi: 10.1002/app.42189.

[75] J. Ren, P. Zhao, W. Liu, and Q. Wu, "Preparation, mechanical, and

thermal properties of biodegradable polyesters/poly(Lactic Acid) blends," *J. Nanomater.*, vol. 2010, 2010, doi: 10.1155/2010/287082.

[76] T. G. Tihan, M. D. Ionita, R. G. Popescu, and D. Iordachescu, "Effect of hydrophilic-hydrophobic balance on biocompatibility of poly(methyl methacrylate) (PMMA)-hydroxyapatite (HA) composites," *Mater. Chem. Phys.*, vol. 118, no. 2–3, pp. 265–269, 2009, doi: 10.1016/j.matchemphys.2009.03.019.

[77] T. Roy, "Preparation and Characterization of nanocomposites Submitted by : Preparation and Characterization of," pp. 4–34, 2014.

[78] R. Scaffaro, A. Maio, F. Sutera, E. ortunato Gulino, and M. Morreale, "Degradation and recycling of films based on biodegradable polymers: A short review," *Polymers (Basel).*, vol. 11, no. 4, 2019, doi: 10.3390/polym11040651.